Catalysis Science & Technology

ROYAL SOCIETY OF CHEMISTRY

PAPER

View Article Online
View Journal | View Issue

Cite this: *Catal. Sci. Technol.*, 2024, 14, 3966

In situ spectroscopic investigations on BiPhePhos modified rhodium complexes in alkene hydroformylation†

Benedict N. Leidecker, [a] Dilver Peña Fuentes, [a] Matthias König, [b] Jiali Liu, [bd] Wolfgang Baumann, [a] Mathias Sawall, [c] Klaus Neymeyr, [ac] Haijun Jiao, [a] Robert Franke, [bd] Armin Börner [a] and Christoph Kubis *[a]

Structural and dynamic properties of BiPhePhos modified rhodium complexes under hydroformylation conditions have been investigated in detail by using high-pressure (HP) *in situ* transmission IR- and NMR-spectroscopy. An experiment design approach which combines component/reagent perturbations, *in situ*-FTIR measurements and chemometric peak group analysis (PGA) led to the identification of most relevant components. The ligand coordination in the structures of the hydrido and acyl 18-VE resting state complexes has been elucidated. The hydrido complex of the type *e,e*-[$HRh(CO)_2(P\cap P)$] represents the dominant resting state after catalyst preformation and during the *n*-regioselective hydroformylation. Dimer formation only takes place to a minor extent under severe reaction conditions under hydrogen depletion. Mono- and dinuclear hydrido monocarbonyl complexes are formed at higher ligand-to-metal ratios and low partial pressures of carbon monoxide. Both stereoisomeric forms of the bisphosphite modified acyl complexes *e,a*-[$RC(O)Rh(CO)_2(P\cap P)$] and *e,e*-[$RC(O)Rh(CO)_2(P\cap P)$] are generated as an equilibrium mixture.

Received 12th April 2024,
Accepted 11th June 2024

DOI: 10.1039/d4cy00481g

rsc.li/catalysis

1. Introduction

Hydroformylation of alkenes to aldehydes is one of the most important homogeneously catalyzed processes in the chemical industry.[1–3] Mononuclear rhodium complexes modified by chelating diphosphites represent a class of highly active, chemo- and regioselective as well as stable catalysts.[4,5] Bidentate diphosphites generally tend to form catalyst complexes for which a lower activity is obtained compared to bulky monophosphites, but the *n*-regioselectivity is often significantly enhanced.[6] Trivalent organic phosphite ligands can undergo several decomposition reactions such as hydrolysis, alcoholysis, *trans*-esterification, Arbuzov rearrangement (alkyl phosphites), O–C bond cleavage, P–O bond cleavage and reactions with aldehydes, depending on the exact ligand structure and reaction conditions.[1,5]

In Scheme 1 a catalytic cycle based on the established Wilkinson-type dissociative mechanism with a rhodium catalyst system modified by a bidentate phosphorus ligand is displayed. Starting from a coordinatively and electronically saturated trigona-bipyramidal 18-valence electron (VE) hydrido complex [$HRh(CO)_2(P\cap P)$] **1**, the dissociation of a carbonyl ligand leads to the formation of a 16 VE hydrido complex **2**, which is planar and has a free coordination site. Complex **2** can activate the alkene substrate under the formation of the π-complex **3**. Two isomeric coordinatively unsaturated alkyl complexes can result from complex **3** by insertion of the alkene into the H–Rh bond. The α-alkyl complex **4** is formed in case of a Rh–C1 bonding, whereas a β-alkyl complex results from a Rh–C2 bonding (**4′**). Eventually the formation of the iso-aldehyde takes place from the β-alkyl complex However, the β-hydride elimination from the secondary alkyl complex might lead to dissociation of the 1-alkene or 2-alkene, which might coordinate again to the catalyst. The coordination of a CO ligand to **4** lead to the coordinatively saturated alky complex **5**. Through the migration of the alkyl group into the Rh–CO bond the planar 16-VE acyl complex **6** is generated. The coordination of a CO ligand forms the 18-VE acyl complex **7**. Product formation might occur *via* oxidative addition of hydrogen to **6** followed by reductive elimination of the aldehyde and regeneration of **2**. This was observed for iridium catalyst systems.[7–9] However, in the literature on rhodium catalyzed hydroformylation the reaction of **6** with molecular hydrogen is also frequently denoted as hydrogenolysis of **6**.[4,10–12] The latter is used in Scheme 1.

[a] *Leibniz Institute for Catalysis e.V., Albert-Einstein Str. 29a, 18059 Rostock, Germany. E-mail: christoph.kubis@catalysis.de*
[b] *Evonik Oxeno GmbH & Co. KG, Paul-Baumann-Str. 1, 45772 Marl, Germany*
[c] *Institute of Mathematics, University of Rostock, Ulmenstr. 59, 18057 Rostock, Germany*
[d] *Lehrstuhl für Theoretische Chemie, Ruhr-Universität Bochum, 44780 Bochum, Germany*

† Electronic supplementary information (ESI) available. See DOI: https://doi.org/10.1039/d4cy00481g

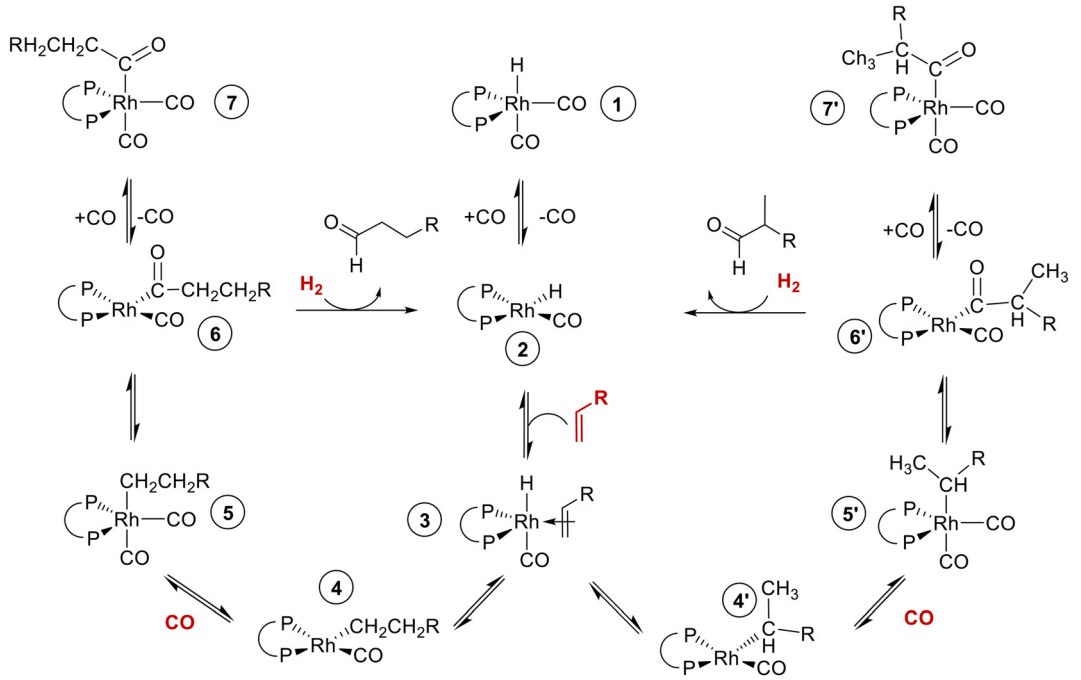

Scheme 1 Catalytic cycle of the chelate-ligand modified rhodium catalysed hydroformylation of alkenes based on a Wilkinson-type mechanism.

For the elucidation of structural and mechanistic aspects *in situ*/operando spectroscopy is performed at real reaction conditions. *In situ* HP FTIR and NMR spectroscopy are powerful techniques which allow for a nearly complete elucidation of molecular structures of catalyst complexes at relevant conditions.[13] FTIR spectroscopy provides distinct spectral patterns for respective transition metal carbonyl complexes. Infrared spectroscopy in the transmission mode is very sensitive and allows for the acquisition of quantitative data in the millimolar and submillimolar concentration range. Complementary structural and dynamic information on catalyst complexes and involved equilibria can be obtained by NMR spectroscopy based on ^{1}H, ^{13}C, ^{31}P and sometimes even ^{103}Rh measurements. Generally higher molar concentrations (5–100 mM) of the catalyst complexes and/or longer acquisition times are needed for an acceptable quality of the NMR spectra. However, higher catalyst concentrations might lead to shifts in chemical equilibria between dissolved transition metal complexes under compressed gases (*e.g.* CO, H_2) because of the varied $[H_2]/[M]$ and $[CO]/[M]$ ratios.

Chemometric data processing tools can extract pure component spectra and corresponding concentration profiles from the collected data set.[14,15] In combination with an experiment design approach based on perturbations, respective algorithms allow for the identification of major, minor and even trace components.[16]

The interpretation of the infrared spectra for transition metal carbonyl complexes can be improved by a vibrational mode analysis based on DFT calculation. Thus, the assignment of vibrational modes even of non-isolable intermediates becomes possible.

Time-resolved *in situ* spectroscopic methods coupled with a simultaneous online-product analysis such as GC or MS permit operando studies from which structure–performance relationships can be derived.

The Rh/BiPhePhos system is a very prominent catalyst for the isomerizing *n*-regioselective alkene hydroformylation (Fig. 1). A hydrido complex of the type $[HRh(CO)_2(P\cap P)]$ is formed *via* an *in situ* formation step treating a solution of the Rh-precursor and diphosphite ligand under synthesis gas (CO/H_2 mixture). Investigations by Moasser, Gladfelter and Roe revealed fundamental insights into the structural and mechanistic aspects of this catalyst system.[17] In succeeding studies by several research groups additional facets such as reaction kinetics as well as catalyst stability were explored in detail.[18–23] Novel separation techniques for molecular catalysts such as TMS (thermomorphic solvent systems) and organic solvent nanofiltration have been developed with the Rh/BiPhePhos catalysts.[24–27] The diphosphite ligand BiPhePhos was also applied in heterogenized catalysts on

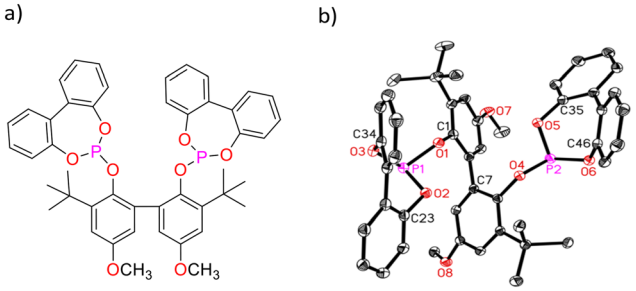

Fig. 1 a) Lewis structural formula of BiPhePhos, b): molecular structure of BiPhePhos (30% probability level, without H).[34]

basis of the SILP (supported ionic liquid phase) and POL (porous organic ligand) concepts.[28–33]

In this present research study new results on the *in situ* spectroscopic characterization of this interesting hydroformylation catalyst in solution based on *in situ* FTIR- and NMR-spectroscopy are presented. After covering the catalytic performance behaviour for selected alkenes, a substantial component identification of the reaction system based on the combination of experiment design by multiple component/reagent perturbations and chemometric analysis of IR-spectroscopic data was carried out. Further, novel aspects on catalyst stability, the coordination of additional ligands to the $[HRh(CO)_2(P\cap P)]$ catalyst and the formation and structure of the corresponding acyl complex $[RC(O)Rh(CO)_2(P\cap P)]$ will be discussed.

2. Results and discussion

2.1 Hydroformylation of alkenes

The hydroformylation of butenes is an industrially relevant process. The formation of valeraldehyde from a mixture of 1-butene, *E*/*Z*-2-butene requires a rhodium catalyst which is active in double bond isomerization as well as in *n*-regioselective hydroformylation. The Rh/BiPhePhos catalyst fulfils the needed properties. Several model reactions with butenes, pentenes and neohexene (Scheme 2) have been performed to demonstrate the potential of this catalyst system at conditions suitable for *in situ* spectroscopic reaction monitoring (Table 1). The reactions were conducted at 90 °C and 2.0 MPa synthesis gas (CO/H_2 = 1 : 1), [Rh] = 1 mM (mmol L^{-1}), [P∩P] = 1 mM, [alkene] = 1 M, solvent: cyclohexane. A transmission flow-through IR-cell with CaF_2 windows and a fixed optical pathlengh of 400 μm was used for the collection of infrared spectra with good signal-to-noise ratios for rhodium concentrations [Rh] ≤ 1 mM. Further details are given in the ESI† (ESI-A).

Prior to the reaction start by the addition of alkene substrate, a preformation of the catalyst is carried out by treating the transition metal precursor $[Rh(acac)(CO)_2]$ with one equivalent of the diphosphite ligand at the same conditions compared to the hydroformylation experiments.

Table 1 Overview of the results from alkene hydroformylation experiments using the Rh/BiPhePhos catalyst

Substrate	Conversion/%	Aldehyde/%	*n*-Regioselectivity[c]/%
1-Butene[a]	>99	>99	>99
2-Butene[a]	>99	>99	>99
1-Pentene[a]	>99	>99	97.5
2-Pentene[a]	>99	>99	97.7
Neohexene[b]	>99	>99	>99

Reaction conditions: $p(H_2)$ = 1.0 MPa, $p(CO)$ = 1.0 MPa, ϑ = 90 °C, [Rh] = 1 mM, [P∩P] = 1 mM, [substrate] = 1 M, solvent: cyclohexane. [a] t = 8 h. [b] t = 4 h. [c] *Via* GC.

1-Butene. The hydroformylation of 1-butene started directly with the addition of alkene without the observation of any induction period (Fig. 2a). The fraction of 1-butene rapidly decreased in the first 10–15 min, after which the concentration of this isomer was below the detection limit of the GC. Corresponding to this the internal butene isomers (*E* and *Z*-2-butene) increased in concentration within this initial interval. This was followed by a succeeding conversion over the entire investigated timespan of 480 min (8 h). Pentanal was the major product with a constant *n*-regioselectivity of >99%. In Fig. 2b the relative molar fraction of the butene isomers *versus* time is displayed. After the addition of 1-butene the composition is altered significantly due to double-bond isomerization.

The momentary content of each isomer is related to its consumption *via* hydroformylation. Thus, the reactivity relation is 1-butene > *Z*-2butene > *E*-2-butene, which is in accordance with their steric properties. The composition of *n*-butenes deviates from the thermodynamic equilibrium composition.[35] The molar fraction of 1-butene after the initial conversion (10–15 min) was below the detection limit and thus lower than the equilibrium value of 0.04. Within the conversion range from 0.10–0.95 the value of *Z*-2-butene decreased from 0.4 to 0.2 (0.26 equilibrium), while the molar fraction of *E*-2-butene increased from 0.6 to 0.8 (0.69 equilibrium). It is important to note that the absolute molar concentrations of the butenes are

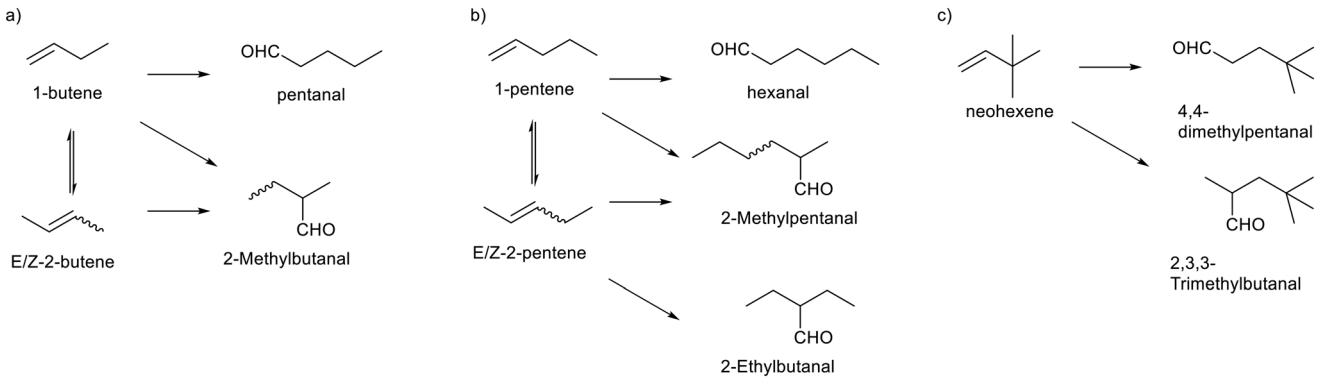

Scheme 2 Isomerization–hydroformylation of a) butene, b) pentene and c) neohexene. Co-substrates CO and H_2 have been left out as well as the catalyst $[HRh(CO)_2(P\cap P)]$ for clarity.

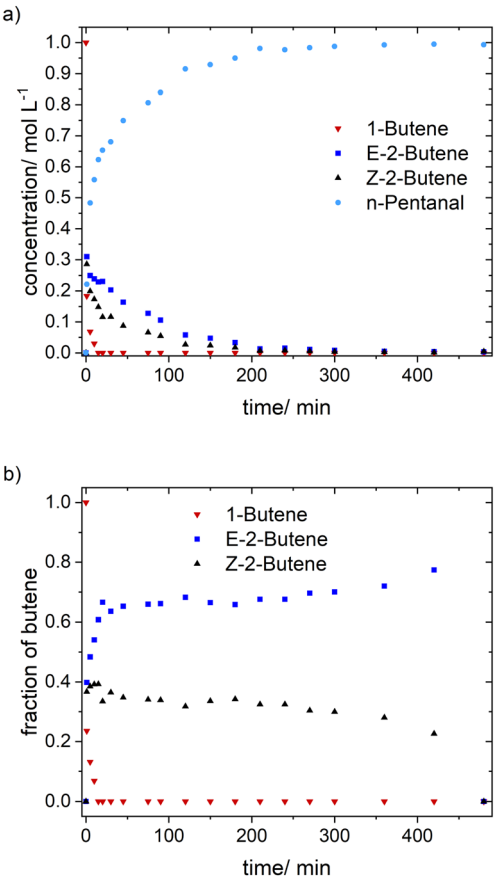

Fig. 2 Concentration profiles of butene isomers and *n*-pentanal obtained for the 1-butene hydroformylation experiment. a) Absolute concentrations *versus* time and b) relative molar fractions of the butene isomers over time. Conditions: [Rh] = 1 mM, [P∩P] = 1 mM, [1-butene] = 1 M, t = 8 h, $p(H_2)$ = 1.0 MPa, p(CO) = 1.0 MPa, ϑ = 90 °C, solvent: cyclohexane.

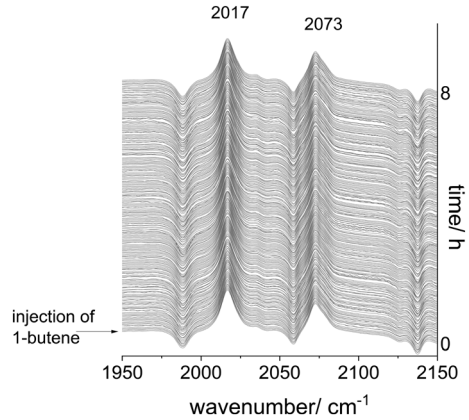

Fig. 3 *In situ* FTIR-spectra measured during 1-butene hydroformylation. Conditions: [Rh] = 1 mM, [P∩P] = 1 mM, [1-butene] = 1 M, t = 8 h, $p(H_2)$ = 1.0 MPa, p(CO) = 1.0 MPa, ϑ = 90 °C, solvent: cyclohexane.

very low at higher conversions. It can be concluded that the isomerization activity is not high enough to equilibrate the *n*-butenes. Formally such type of reaction system can be classified as coupled parallel reaction.[36]

Based on the *in situ* FTIR spectroscopic monitoring the hydrido complex [$HRh(CO)_2$(P∩P)] (ν(CO) = 2017, 2073 cm^{-1}) was the only detectable rhodium species over the entire conversion range in accordance with other studies on hydroformylation with diphosphite modified rhodium catalysts (Fig. 3).[6,21,37]

2-Butenes. The hydroformylation of an equimolar mixture of *Z*- and *E*-2-butene showed the formation of small portions of 1-butene within the first 45 min resulting in a molar fraction of 0.01 (equilibrium 0.04), see ESI-C.† After this time period no 1-butene was detectable anymore *via* GC. Directly after addition of the 2-butene mixture *E*-2-butene was accumulated up to 0.6 (equilibrium 0.69) and the fraction of *Z*-2-butene was consumed to 0.39 (equilibrium 0.27). The composition of the 2-butene isomers remained almost unchanged over a large conversion range but showed a significant alteration from 210 min onwards, with an enrichment of the less reactive *E*-2-butene to 0.8. Depletion of *Z*-2-butene over the course of the reaction time indicate the key role of this more reactive isomer in the double bond isomerisation towards 1-butene followed by the consecutive hydroformylation to *n*-pentanal. The hydrido complex [$HRh(CO)_2$(P∩P)] was the only observable species during the reaction. Further details and graphical representations of the data are given in the ESI-C.†

1-/2-Pentenes. The hydroformylation of 1-pentene and a mixture of 2-pentenes ($Z:E$ = 0.29 : 0.71) showed a similar behavior regarding the composition of *n*-pentene molar fractions during the reaction compared with the butene experiments. In both cases the fraction of 1-pentene (0.02) was only slightly lower than the value for the equilibrium composition (0.03). The fraction of the less reactive *E*-2-pentene increased to 0.8 (0.63 equilibrium) over the observed time while for the more reactive *Z*-2-pentene dropped to a value of 0.2 (equilibrium 0.33). Simultaneous *in situ* spectroscopic monitoring revealed that only the hydrido complex was detected over the entire conversion range. Figures of the acquired experimental data are given in ESI-C.†

Neohexene. The substrate neohexene (3,3-dimethyl-1-butene) was also chosen because it is incapable for double-bond isomerization and is often used for kinetic and spectroscopic studies. Hydroformylation of neohexene proceeds with an apparent first order kinetics with respect to the substrate concentration (k^{obs} = 0.04 min^{-1}) (Fig. 4a). The reaction reaches full conversion within 3 hours and is highly chemo- and *n*-regioselective forming 4,4-dimethylpentanal as the only product. Furthermore, the *in situ* FTIR-spectroscopy proves the exclusive presence of [$HRh(CO)_2$(P∩P)] as only observable catalyst species during the hydroformylation (Fig. 4b).

2.2 Component identification based on experiment design and peak group analysis (PGA) of spectroscopic data

In this section the results from a single *in situ* FTIR experiment with stepwise additions of reactants aimed for the identification of all relevant components of the reaction system consisting of

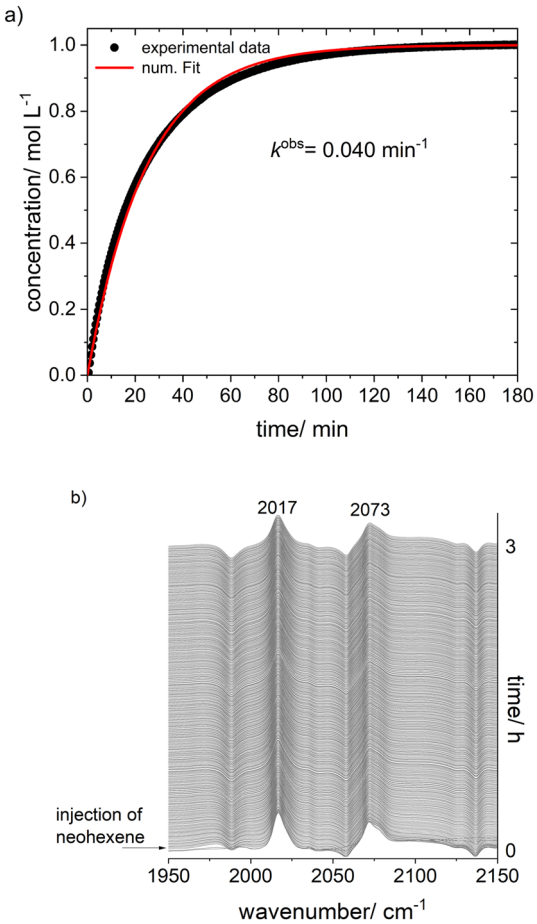

Fig. 4 Neohexene hydroformylation using Rh/BiPhePhos catalyst. a) Concentration profile of 4,4-dimethyl-1-butene formation, b) *in situ* FTIR-spectra of the carbonyl region. Conditions: [Rh] = 1 mM, [P∩P] = 1 mM, [neohexene] = 1 M, t = 3 h, $p(H_2)$ = 1.0 MPa, p(CO) = 1.0 MPa, ϑ = 90 °C, solvent: cyclohexane.

rhodium complexes and organic compounds are discussed. The sequential dosage of reactants at distinct intervals under continuous measurement of time-resolved infrared spectra can lead to data sets suitable for the extraction of pure component spectra using chemometric tools such as the peak group analysis (PGA).[38,39] Scheme 3 gives an overview about the dosage sequence used in this experiment and in Fig. 5 the entire data set of collected infrared spectra are displayed.

The solvent cyclohexane, stock solutions of diphenyl carbonate as internal IR standard and BiPhePhos were injected one after the other into the reactor system (ESI-D†). Infrared spectra were registered continuously in each step within a time interval of 10 min. In the next step the reactor was charged with 2.0 MPa synthesis gas (CO/H_2 = 1 : 1) after which the stock solution of Rh precursor [Rh(acac)$(CO)_2$] was dosed using a syringe pump. This initiated the preformation of the hydride complex [$HRh(CO)_2$(P∩P)] which was completed after *ca.* 60 min. Then, a gas-exchange for 1.0 MPa deuterium and 1.0 MPa carbon monoxide was performed to form the corresponding deuteride complex. After a repeated gas-exchange to hydrogen/carbon monoxide and then pure CO, the system was pressurized with 1.0 MPa ethene to generate acyl complexes. Due to the small size of ethene the formation of observable acyl complexes is favored under pure CO conditions.

The entire infrared spectroscopic data set was processed by the peak group analysis tool (PGA) from the FACPACK package.[38–40] Peak group analysis (PGA) is a chemometric approach using Multivariate Curve Resolution (MCR) techniques to extract pure component spectra from spectral mixture data. PGA works incrementally, starting with a single peak for which it constructs the associated pure component spectrum that reproduces that peak. This process is repeated for all dominant peaks in the measured data. The resulting series of potential pure component spectra is subjected to correlation analysis to identify groups of very similar spectra. Ideally, the resulting distinct groups of spectra can be related to the pure component spectra of the reactive species.

The extracted pure component spectra are presented in Fig. 6a. There are only very minor artefacts present in the spectrum. Due to the sequential dosage experiment design linear dependencies in the data matrix related to spectra and/or concentration profiles can often be removed to a significant extent. In Fig. 6b the obtained spectra of the different rhodium complexes in an enlarged size are displayed showing detailed spectral features of the distinct components. The interpretation of the vibrational patterns and assignments to molecular structures are discussed in the following sections.

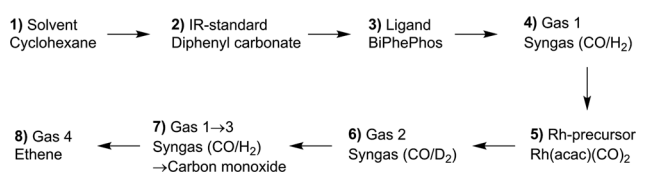

Scheme 3 Sequence for the stepwise dosage experiment. Time interval between the steps was 10 min. Further reaction conditions: ϑ = 50 °C, [Rh] = 1 mM, [P∩P] = 1 mM, [DPC] = 1 mM, P(syngas) = 2.0 MPa, p(ethene) = 1.0 MPa.

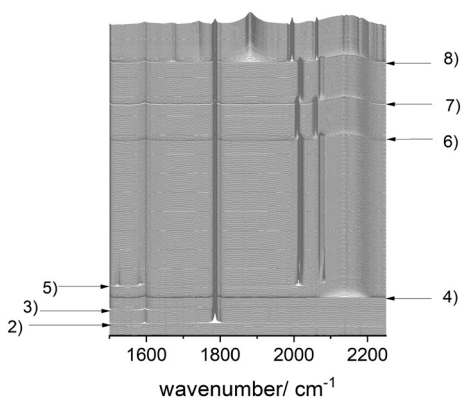

Fig. 5 *In situ* spectroscopic IR-data of a sequential dosage experiment. Conditions: [Rh] = 1 mM, [P∩P] = 1 mM, [DPC] = 2 mM, $p(H_2/D_2)$ = 1.0 MPa, p(CO) = 1.0 MPa, $p(C_2H_4)$ = 1.0 MPa, ϑ = 50 °C, solvent: cyclohexane.

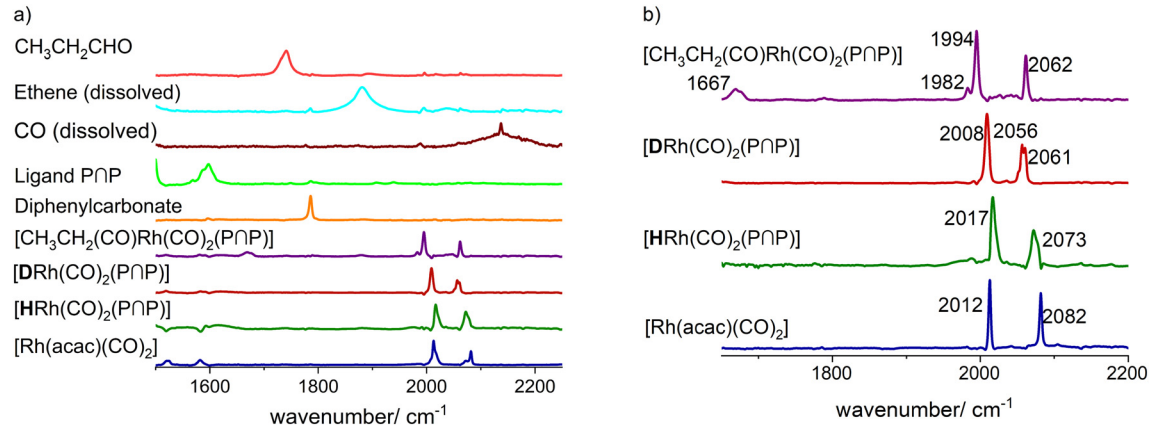

Fig. 6 a) Extracted pure component spectra from the PGA processing of collected *in situ* spectroscopic IR-data of a sequential dosage experiment, b) selection of extracted spectra for rhodium carbonyl complexes (enlarged view). Conditions: [Rh] = 1 mM, [P∩P] = 1 mM, [DPC] = 2 mM, $p(H_2/D_2)$ = 1.0 MPa, $p(CO)$ = 1.0 MPa, $p(C_2H_4)$ = 1.0 MPa, ϑ = 50 °C, solvent: cyclohexane.

2.3 Spectroscopic characterization of [Rh(acac)(P∩P)]

The treatment of the rhodium precursor [Rh(acac)$(CO)_2$] with one equivalent of BiPhePhos ligand forms the respective complex [Rh(acac)(P∩P)] under the evolution of gaseous carbon monoxide (Scheme 4). This is caused by the chelating coordination of the phosphorus atoms of BiPhePhos and substitution of the carbonyl ligands. Depending on the conditions, *e.g.* rhodium concentration and ligand-to-metal ratio, a certain amount of the monocarbonyl [Rh(acac)(CO)(κ^1-P∩P)] can also be formed (see further below).

The infrared spectroscopic monitoring of this substitution reaction at [Rh] = 1 mM and [P∩P]/[Rh] = 1 shows the complete vanishing of the vibrational bands for the carbonyl ligands of [Rh(acac)$(CO)_2$] (ν(CO) = 2012, 2082 cm^{-1}) (Fig. 7a). Another observation is a slight shift of the positions for the vibrational bands of the acetylacetonate ligand ($acac^-$): [Rh(acac)$(CO)_2$] (ν(acac) = 1528, 1582 cm^{-1}) → [Rh(acac)(P∩P)] (ν(acac) = 1520, 1584 cm^{-1}). Such a shift is also in line with DFT-based vibrational spectra (Fig. 7b) and is characteristic for the coordination of phosphite ligands to the precursor.

At higher rhodium concentrations ([Rh] = 20 mM) a band at ν(CO) = 2008 cm^{-1} with low intensity was observed which indicates the presence of [Rh(acac)(CO)(κ^1-P∩P)] at comparatively low concentrations (Fig. 7a and b).

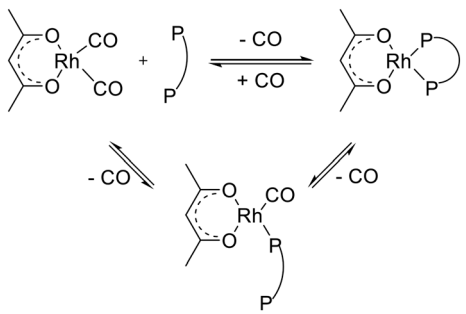

Scheme 4 Formation of [Rh(acac)(P∩P)] starting from [Rh(acac)$(CO)_2$] and BiPhePhos (P∩P). The monocarbonyl complex [Rh(acac)(CO)(κ^1-P∩P)] can be formed which highly depends on the reaction conditions.

NMR spectroscopy on solutions with a rhodium concentration of 20 mM ([P∩P]/[Rh] = 1) allowed for the detection of the characteristic ^{31}P doublet signals at $\delta(^{31}P)$ = 146.3 ppm (d, $^1J_{P,Rh}$ = 293 Hz) for [Rh(acac)(P∩P)] as the

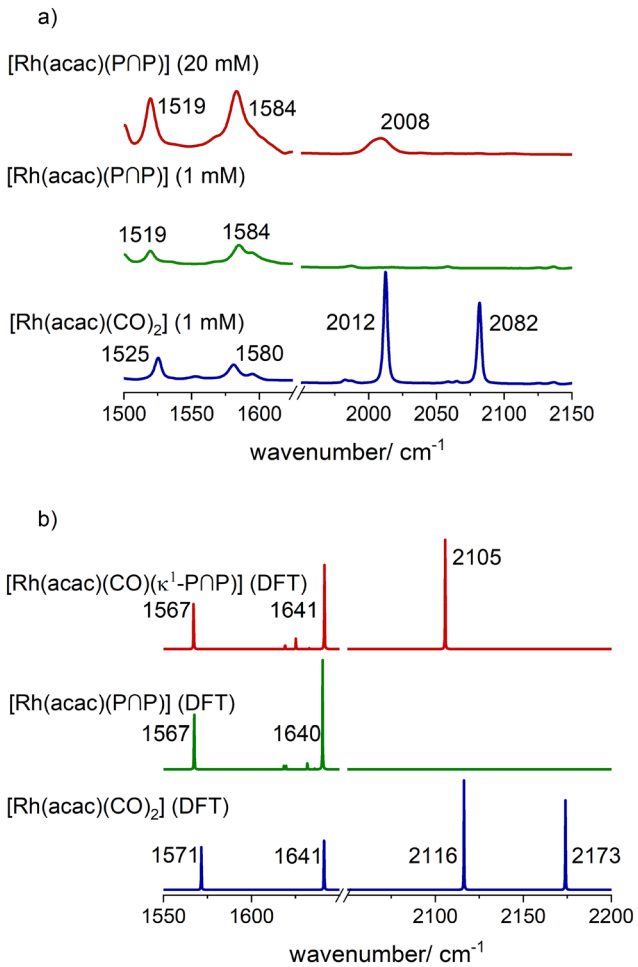

Fig. 7 a) *In situ* IR-spectra of [Rh(acac)$(CO)_2$] and [Rh(acac)(P∩P)] and b) DFT-based vibrational spectra (ESI-I†). Conditions: [Rh] = 1 mM, [P∩P] = 1 mM, p(Ar) = 0.1 MPa, ϑ = 30 °C, solvent: cyclohexane.

major complex and $\delta(^{31}P)$ = 140.3 Hz (d, $^{1}J_{P,Rh}$ = 283 Hz) for the minor monocarbonyl complex [Rh(acac)(CO)(κ^1-P∩P)] with *ca.* 6% of the signal intensity (Fig. 8).[17,41] The signal for the uncoordinated phosphite unit is expected to resonate between *ca.* 146–150 ppm which overlaps with the signal of [Rh(acac)(P∩P)]. The integral values for both parts of the doublet signal centered at 146.3 ppm are not identical and the difference compares approximately to the integral value of the signal at 140.3 ppm (ESI-B†). In addition, a $^{31}P\{^{1}H\}$–^{103}Rh-HMBC spectrum was measured which gave a single ^{103}Rh-NMR signal at $\delta(^{103}Rh)$ = 140 ppm for [Rh(acac)(P∩P)] which indicates that only one rhodium atom is coordinated in the complex. Further signals were observed at $\delta(^{103}Rh)$ = 223 ppm for [Rh(acac)(CO)(κ^1-P∩P)] and $\delta(^{103}Rh)$ = 215 ppm for a low amount of the precursor [Rh(acac)$(CO)_2$].

2.4 *In situ* formation of [HRh$(CO)_2$(P∩P)]

The treatment of [Rh(acac)(P∩P)] ([Rh] = 1 mM) with synthesis gas (H_2/CO, 2.0 MPa) at ϑ = 50 °C to generate a corresponding hydrido complex (Scheme 5) was investigated by *in situ* FTIR spectroscopy. After the addition of synthesis gas the bands assigned to the dicarbonyl complex [Rh(acac)$(CO)_2$] (ν(CO) = 2012, 2082 cm^{-1}) appeared immediately followed by an ongoing increase of bands assigned to [HRh$(CO)_2$(P∩P)] (ν(CO) = 2017, 2073 cm^{-1}) (Fig. 9). The reaction was complete after *ca.* 50 min. A rapid partial substitution of the phosphorus atoms of the coordinated ligand by carbon monoxide at elevated pressures is a known behaviour for many diphosphites. The generation of acetylacetone in course of the hydrogenolysis of [Rh(acac)$(CO)_2$] could not be observed clearly by IR-spectroscopy at this concentration.

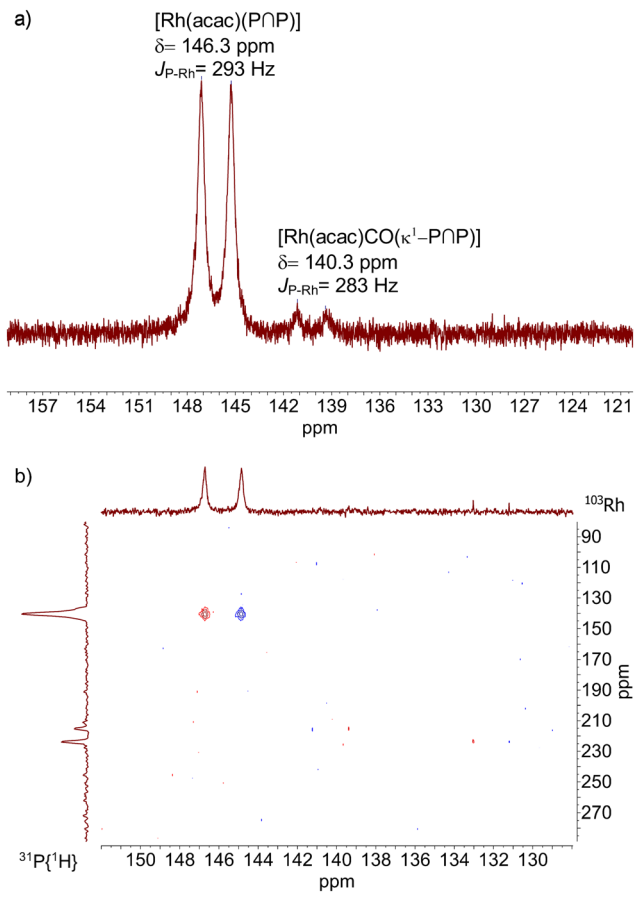

Fig. 8 a) $^{31}P\{^{1}H\}$-NMR-spectrum of [Rh(acac)(P∩P)] and b) $^{31}P\{^{1}H\}$–^{103}Rh-NMR of [Rh(acac)(P∩P)]. Conditions: [Rh] = 20 mM, [P∩P] = 20 mM, p(Ar) = 0.1 MPa, ϑ = 25 °C, solvent: toluene-d_8; spectrum b) was acquired at ϑ = 30 °C.

For the elucidation of the coordination mode of the P-atoms in the hydrido dicarbonyl complex an *in situ* IR experiment with isotopic labeling (H/D-exchange) was performed (Fig. 10a). For further assignments of the IR-bands to vibrational modes DFT calculations based on trigonal-bipyramidal hydrido complex structures in which the hydride ligand is located in the axial position with bis-equatorial and equatorial–axial coordination of the P-ligand have been conducted (Fig. 10b and c). A shift of the respective IR-bands in the experimental spectrum of the deuterido complex to lower wavenumbers have been observed: [DRh$(CO)_2$(P∩P)] (ν(CO) = 2009, 2058 cm^{-1}). Such a band shift is in agreement with a bis-equatorial coordination of the P-atoms.[17,42–44] Since there is a H–Rh–CO *trans*-arrangement in the *e*,*e*-[HRh$(CO)_2$(P∩P)] complex the isotopic labeling with deuterium affects the corresponding combined vibrational modes (vibrational modes for an idealized geometry *e*,*e*-[HM$(CO)_2L_2$] ((C_s) → 2A′)). This is proven by the vibrational mode analysis based on DFT calculations. In the stereoisomer *e*,*a*-[HRh$(CO)_2$(P∩P)] there are only H–Rh–CO *cis*-arrangements, therefore an H/D-exchange does not lead to any shift of respective carbonyl bands in the infrared spectrum (vibrational modes for an idealized geometry *e*,*a*-[HM$(CO)_2L_2$] ((C_s) → A″ + A′)). The observed preferred formation of the *e*,*e*-[HRh$(CO)_2$(P∩P)] stereoisomer is also in agreement with relative energies calculated by DFT computations (ESI-J†).

The results from an NMR-spectroscopic characterization of the hydrido complex in solution are in good accordance with the IR-spectroscopic data. Sample preparation was conducted in a 10 mL stainless steel cylinder with following conditions: [Rh] = 20 mM, [P∩P] = 20 mM, p(syngas) = 2.0 MPa, ϑ = 50 °C, t = 2 h in toluene-d_8. The solution was purged with Ar and transferred after the preformation into a Young-NMR tube and measured at ϑ = 25 °C. The stability of the hydrido complex at one atmosphere of the mixture of hydrogen and carbon monoxide has been tested in a previous control experiment and is discussed further below. In the ^{1}H-NMR spectrum a characteristic signal in the hydride region at $\delta(^{1}H)$ = −10.6 ppm (dd, $^{1}J_{H,P}$ = 8.3 Hz, $^{1}J_{H,Rh}$ = 3.5 Hz) is observed (Fig. 11a). The small value of the coupling constant $^{1}J_{H,P}$ = 8.3 Hz indicates a *cis*-phosphorus-hydride coordination with only a slight distortion of the tbp complex.[6,17,41,44–46] A ^{1}H–^{103}Rh-HMBC experiment was also conducted giving a signal at $\delta(^{103}Rh)$ = −1146 ppm and the respective cross signals (Fig. 11b). The $^{31}P\{^{1}H\}$-NMR

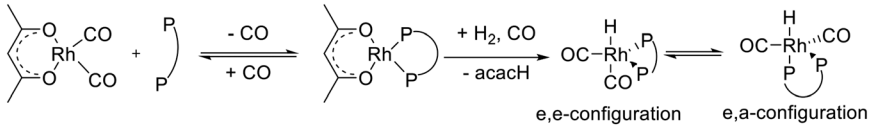

Scheme 5 Reaction of [Rh(acac)(CO)$_2$] with BiPhePhos (P∩P) towards possible stereoisomeric hydrido complexes.

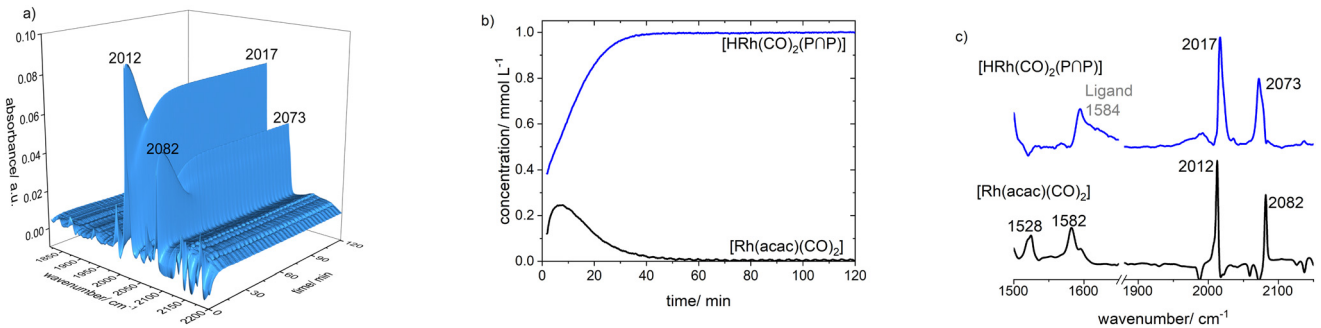

Fig. 9 a) *In situ* IR-spectra from the catalyst formation in dependency of the time; b) concentration profiles and c) pure component spectra from the peak group analysis (PGA) of IR-spectroscopic data. Conditions: [Rh] = 1 mM, [P∩P] = 1 mmol, p(CO) = 1.0 MPa, p(H$_2$) = 1.0 MPa, ϑ = 50 °C, solvent: cyclohexane.

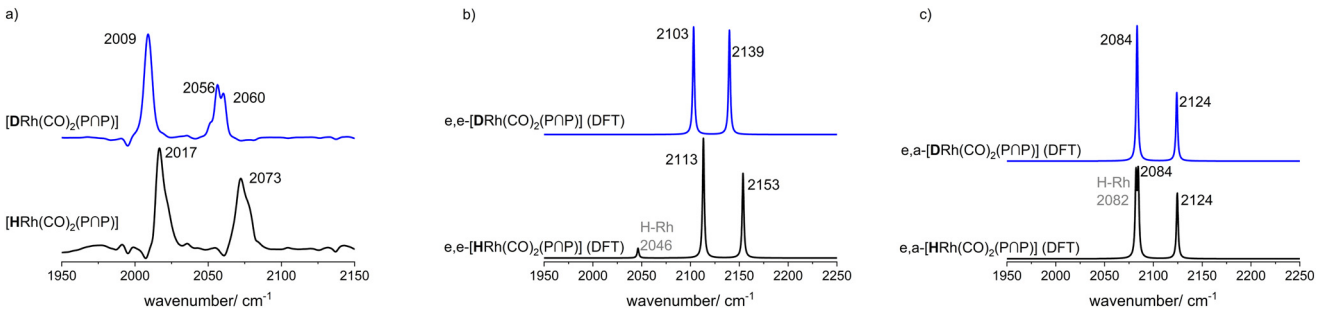

Fig. 10 a) IR spectroscopic data from H/D-exchange experiment on [H/DRh(CO)$_2$(P∩P)] conditions: [Rh] = 1 mM, [P∩P] = 1 mM, p(CO) = 1.0 MPa, p(H$_2$/D$_2$) = 1.0 MPa and DFT-based IR-spectra (ESI-I†) of the H/D-exchange for b) *e,e*-complex and c) *e,a*-coordination of the ligand. Colours: black: hydrido, blue: deuteride complex.

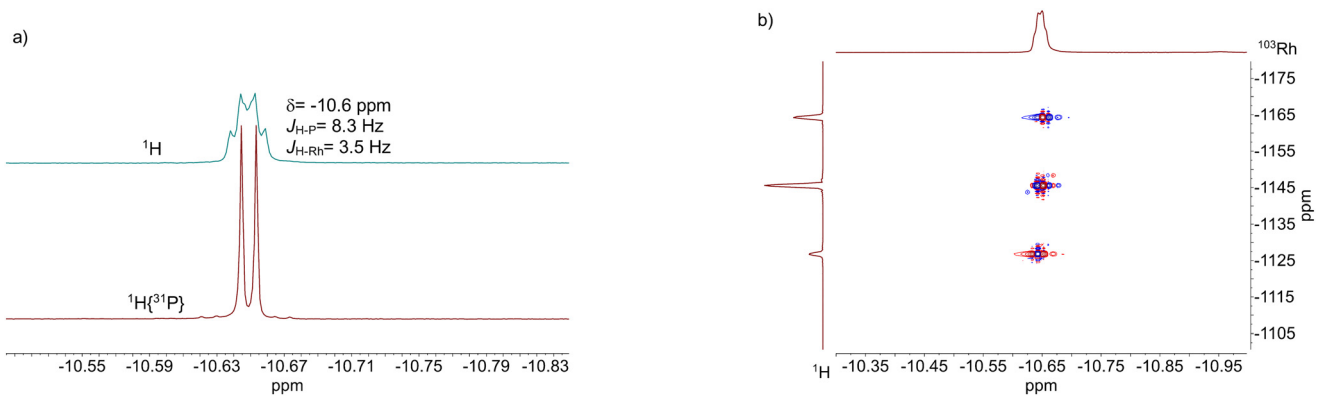

Fig. 11 a) ^{1}H-NMR and ^{1}H{^{31}P}-NMR and b) ^{1}H–^{103}Rh-HMBC spectrum of [HRh(CO)$_2$(P∩P)]. Conditions: [Rh] = 20 mM, [P∩P] = 20 mM, p(Ar) = 0.1 MPa, ϑ = 25 °C, solvent: toluene-d$_8$.

spectrum reveals a doublet signal at δ(^{31}P) = 174.0 ppm (d, $^1J_{P,Rh}$ = 237 Hz) and the ^{31}P{^{1}H}–^{103}Rh-HMBC spectrum confirms the presence of a mononuclear Rh(I) complex (Fig. 12). ^{13}C{^{1}H}-NMR spectroscopy was performed on a ^{13}CO-labeled (labeling degree ^{13}CO: 50%) sample of the dissolved hydrido complex with [Rh] = 20 mM, [Rh]/[P∩P] = 1. We assigned the signals at room temperature (297 K) to an averaged doublet of triplet resonance δ(^{13}C) = 194.6 ppm (dt,

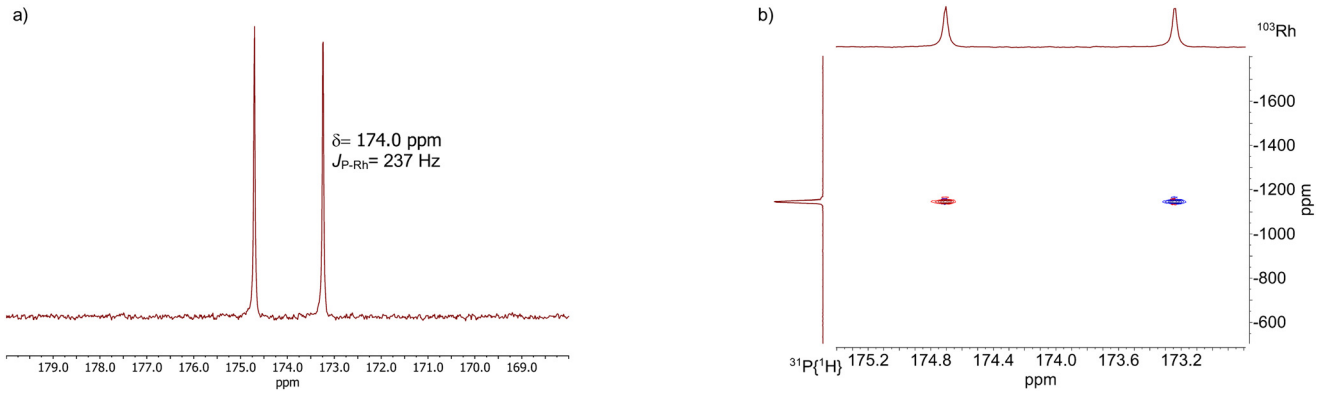

Fig. 12 a) ^{31}P{^{1}H}-NMR of [HRh(CO)$_2$(P∩P)] and b) ^{31}P{^{1}H}–^{103}Rh-HMBC spectrum (no decoupling) of [HRh(CO)$_2$(P∩P)]. Conditions: [Rh] = 20 mM, [P∩P] = 20 mM, p(CO) = 0.05 MPa, p(H$_2$) = 0.05 MPa, ϑ = 25 °C, solvent: toluene-d$_8$.

$^{1}J_{C,Rh}$ = 58.8 Hz, $^{2}J_{C,P}$ = 15.9 Hz) which corresponds to both carbonyl ligands (Fig. 13). Cooling to −60 °C (213 K) led to signal broadening. Thus, in the investigated temperature range the positions of the two carbonyl ligands are not fixed and their coordination modes could not be distinguished. Isotope effects on the shifts of ^{1}H, ^{31}P and ^{103}Rh due to the ^{13}CO labelling were detected (ESI-E†). Five-coordinate trigonal bipyramidal complexes of the type [HRh(CO)$_2$(P∩P)] often show fluxional behavior. Intramolecular rearrangement processes are described in the literature.[46–50] With respect to the carbonyl ligands also intermolecular exchange between coordinated and uncoordinated carbon monoxide might be involved.[51,52] Based on the present data, no discrimination of the exact exchange mechanism is possible. A series of additional experiments would be required which go beyond the framework of the present study.

2.5 Stability aspects of [HRh(CO)$_2$(P∩P)]

Catalyst stability is a crucial issue with respect to industrial applicability and economic efficiency of a catalytic system.[5,23,53,54] For diphosphite modified rhodium complexes as hydroformylation catalysts the formation of dimers and polynuclear clusters might take place at low partial pressures of hydrogen and carbon monoxide.

To study the behaviour of [HRh(CO)$_2$(P∩P)] in the absence of hydrogen and carbon monoxide, we performed an *in situ* IR experiment under pure inert gas at 90 °C for 9 h. The hydrido complex was generated at [Rh] = 1 mM and [P∩P]/[Rh] = 1 during the treatment with synthesis gas at 50 °C for 1 h. Then, the synthesis gas was thoroughly purged with argon (5 times gas exchange from 1.0 MPa argon → 0.1 MPa). The solution was monitored by IR-spectroscopy at 90 °C and 1.0 MPa of argon. There were no alterations in the infrared spectra within the timespan of 9 h (Fig. 14), which indicates an intrinsically good stability of the hydrido complex under inert atmospheres depleted of hydrogen and carbon monoxide.

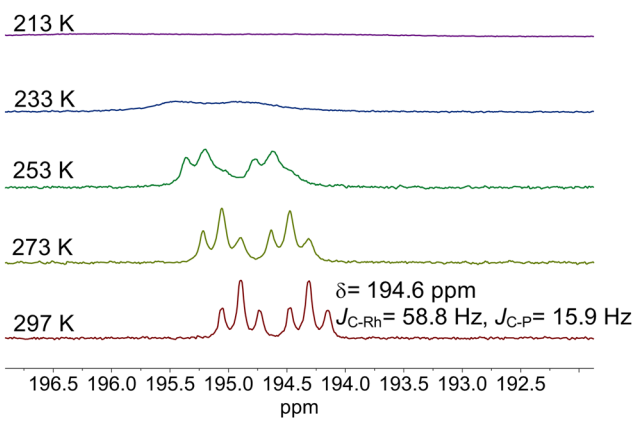

Fig. 13 ^{13}C{^{1}H}-NMR spectra of [HRh(CO)$_2$(P∩P)] after isotopic labeling with 50% ^{13}CO under variation of the temperature. Conditions: [Rh] = 20 mM, [P∩P] = 20 mM, p(^{12}CO) = 0.025 MPa, p(^{13}CO) = 0.025 MPa, p(H$_2$) = 0.05 MPa, solvent: toluene-d$_8$.

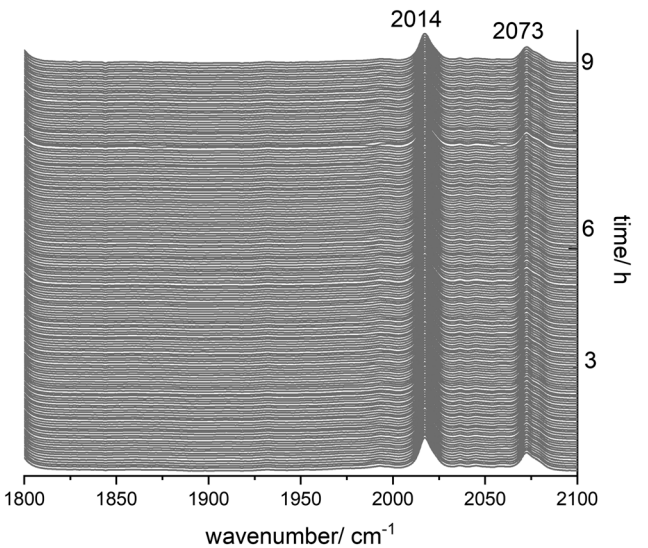

Fig. 14 *In situ* IR-spectroscopic data from the stability test of [HRh(CO)$_2$(P∩P)] under an Ar atmosphere. Conditions: [Rh] = 1 mM, [P∩P] = 1 mM, p(Ar) = 1.0 MPa, ϑ = 90 °C, solvent: cyclohexane.

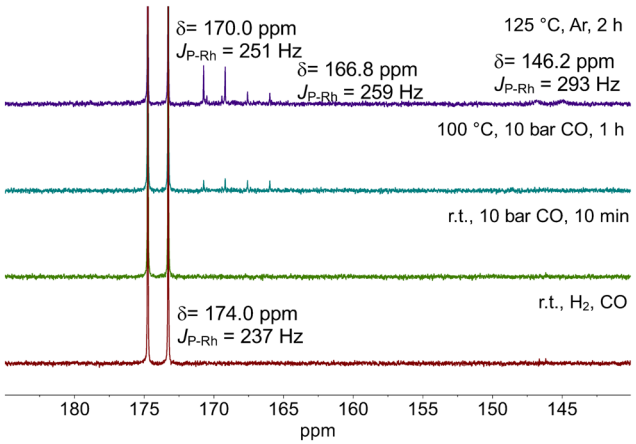

Fig. 15 $^{31}P\{^1H\}$-spectra of $[HRh(CO)_2(PP)]$ under syngas, CO and Ar at varying temperatures. Further conditions: [Rh] = 20 mM, [P∩P] = 20 mM, p = 0.1 MPa, solvent: toluene-d_8.

Further experiments have been performed on a solution of the hydrido complex at higher rhodium concentrations ([Rh] = 20 mM and [P∩P]/[Rh] = 1, solvent: toluene-d_8) analyzed by NMR-spectroscopy. After the formation of the hydrido complex at 100 °C and 2.0 MPa of synthesis gas, we released the pressure to 0.1 MPa and transferred the sample into the NMR tube. The $^{31}P\{^1H\}$-NMR spectrum displayed the doublet signal characteristic for $[HRh(CO)_2(P\cap P)]$ at $\delta(^{31}P)$ = 174.0 ppm (d, $^1J_{P,Rh}$ = 237 Hz) without any additional signals (Fig. 15).

The removal of dissolved hydrogen by pure CO did not lead to any changes in the NMR spectrum. However, after the treatment under 1.0 MPa of carbon monoxide at 100 °C tiny signals at $\delta(^{31}P)$ = 170.0 ppm (m, $^1J_{P,Rh}$ = 251 Hz) and $\delta(^{31}P)$ = 166.8 ppm (m, $^1J_{P,Rh}$ = 259 Hz) appeared indicating the formation of isomeric forms of a dinuclear complex of the type $[Rh_2(CO)_4(P\cap P)_2]$.[17] The intensity of these signals further increased after the solution was further treated in inert gas (argon) at 125 °C for 2 h. In addition, a doublet signal at $\delta(^{31}P)$ = 146.2 ppm (d, $^1J_{P,Rh}$ = 293 Hz) was detected which belongs to [Rh(acac)(P∩P)]. In total, *ca.* 9% of the signal intensity in the ^{31}P-NMR spectrum correspond to the dinuclear complexes and *ca.* 6% to the precatalyst complex.

Catalyst decomposition in the presence of air. The lability of transition metal complexes as catalysts towards oxygen and oxidants is an important aspect.[55] The impact of the addition of air on the hydrido complex $[HRh(CO)_2(P\cap P)]$ was studied by *in situ* IR-spectroscopy. The catalyst complex was generated by the preformation at standard conditions ([Rh] = 1 mM, [P∩P] = 1 mM, $p(CO/H_2)$ = 2 MPa, ϑ = 50 °C, t = 2 h). In the next step 0.3 MPa of air was added at three temperatures: ϑ = 30 °C, 50 °C and 90 °C. At 30 °C and 50 °C no decomposition of the hydrido complex was observed during the treatment for 90 min. In the course of treatment with air at 90 °C a significant decrease of the bands assigned to $[HRh(CO)_2(P\cap P)]$ (ν(CO) = 2017, 2070 cm^{-1}) was detected connected with an evolution of the bands attributed to $[Rh(acac)(CO)_2]$ (ν(CO) = 2012, 2082 cm^{-1}) (Fig. 16). This indicates indirectly also a degradation of the ligand BiPhePhos because otherwise the formation of [Rh(acac)(P∩P)] would be expected.

Stability of BiPhePhos and $[HRh(CO)_2(P\cap P)]$ against water. Phosphites are known to be prone towards hydrolytic decomposition.[56,57] We performed test NMR-experiments to investigate the lability of BiPhePhos and $[HRh(CO)_2(P\cap P)]$ in the presence of water. Formation of $[HRh(CO)_2(P\cap P)]$ was conducted at the following conditions: [Rh] = 20 mM, [P∩P] = 20 mM, $p(CO/H_2)$ = 2 MPa, ϑ = 50 °C, t = 2 h, solvent: 1,4-dioxane. 1,4-Dioxane was chosen as a solvent due to its miscibility with water. Afterwards, the solution was transferred into a 20 mL Schlenk tube, and 20 eq. of water were added. A solution of BiPhePhos was prepared under the same conditions ([P∩P] = 20 mM, [H_2O] = 400 mM). Both solutions were heated up to ϑ = 90 °C and at distinct time-points NMR-samples (0.6 mL) were taken out and subsequently measured by NMR spectroscopy (ESI-E†).

Based on quantitative ^{31}P-NMR spectroscopic data (Fig. 17) both samples showed a slight decrease in the fraction of the total ^{31}P-integral of each component (0.97 initial value) directly after the addition of water: 0.87 (hydrido complex) and 0.94 (BiPhePhos).

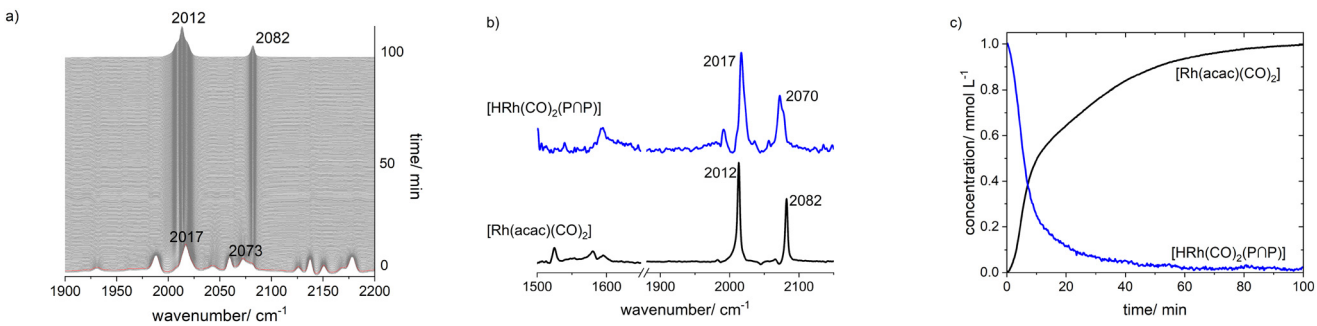

Fig. 16 *In situ* IR-spectra series of the reaction of $[HRh(CO)_2(P\cap P)]$ with air, b) pure component spectra extracted from a), c) corresponding relative absorbance profiles extracted with the peak group analysis. Conditions: [Rh] = 1 mM, [P∩P] = 1 mM, p(air) = 0.3 MPa, ϑ = 90 °C, t = 90 min, solvent: cyclohexane.

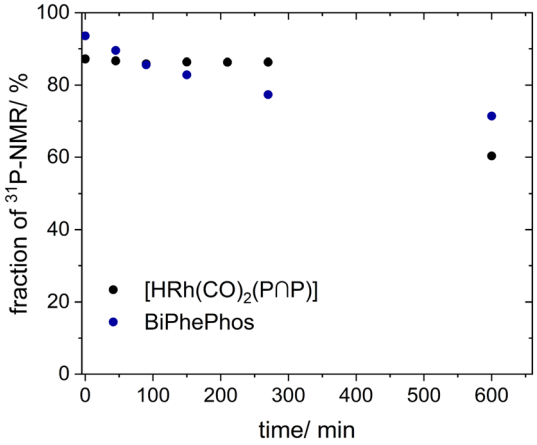

Fig. 17 Hydrolysis control test. Integral fractions for [HRh(CO)$_2$(P∩P)] (black) and BiPhePhos (blue) based on quant. ^{31}P{^{1}H}-spectra. Further conditions: [Rh] = 20 mM, [P∩P] = 20 mM, [H$_2$O]/[P∩P] = 20, p = 0.1 MPa, solvent: 1,4-dioxane.

While the fraction of [HRh(CO)$_2$(P∩P)] remained almost constant throughout the course of the first 270 min, the fraction of BiPhePhos sample showed a succeeding decrease to 0.77 after 270 min. Longer treatments until 600 min led to an accelerated decomposition of [HRh(CO)$_2$(P∩P)] (0.60) which might indicate an autocatalytic pathway.[56,57] Such an enhanced decay was not clearly observed for BiPhePhos (0.71) within the examined time span.

2.6 Influence of the ligand-to-metal ratio on the composition of hydrido complexes

The bulkiness of a chelating diphosphite such as BiPhePhos has a tremendous impact on the molecular structure and catalytic properties of the corresponding hydrido complex. As it is outlined in this study, the P-atoms of the ligand BiPhePhos coordinate in a bis-equatorial mode in *e*,*e*-[HRh(CO)$_2$(P∩P)] for ([P∩P]/[Rh] = 1). The coordination chemistry at larger ligand-to-metal ratios has not been described in detail in the literature so far, thus we performed comparative *in situ* infrared and NMR experiments for [P∩P]/[Rh] = 1, 1.5 and 2.

A solution of [HRh(CO)$_2$(P∩P)] ([Rh] = 1 mM) was prepared in the presence of the respective amount of BiPhePhos at p(CO/H$_2$) = 2.0 MPa and ϑ = 90 °C. It is to be noticed that at elevated pressures of synthesis gas (2.0 MPa) only the infrared bands assigned to the hydrido complex were identified (Fig. 18a). During repeated gas exchange cycles (up to 12 times) with pure hydrogen, an additional band at ν(CO) = 2045 cm^{-1} increased until its intensity reached a constant value (Fig. 18b). As expected, the molar fraction of the putative monocarbonyl complex seems to be higher for [P∩P]/[Rh] = 2. The latter experiment was repeated for [Rh] = 20 mM in toluene-d$_8$ (Fig. 18c) which was also used for NMR-measurements. Based on the IR-spectra the trends with respect to the population of the mononuclear complex was similar when comparing the two concentration levels of rhodium.

^{1}H{^{31}P}- and ^{31}P{^{1}H}-NMR spectra revealed that depending on the ligand-to-metal ratio different types of hydrido complexes were formed (Fig. 19). For [P∩P]/[Rh] = 1.5 besides the typical doublet signal for [HRh(CO)$_2$(P∩P)] (δ(^{1}H) = −10.6 ppm) several additional resonances in the hydride region of the ^{1}H{^{31}P}-NMR spectrum were present. In the ^{31}P{^{1}H}-NMR spectrum in addition to the doublet signal for the hydrido dicarbonyl complex (δ(^{31}P) = 174.0 ppm) very complex coupled multiplet patterns for coordinated phosphite moieties were observed. But the spectra were without any signals in the region of uncoordinated P-atoms. Together with the results from IR-spectroscopy in which the formation of a monocarbonyl complex was observed, the spectroscopic data would be in agreement with a ligand bridging dinuclear complex of the type [HRh(CO)(P∩P)]$_2$(P∩P) (Scheme 6).[58,59] Interestingly, for [P∩P]/[Rh] = 2 new additional hydride signals were detected in the proton NMR spectrum. In the ^{31}P-NMR spectrum also a complex multiplet pattern in the region of coordinated P-atoms was seen with additional signals in the regions of non-coordinated phosphite ligands.

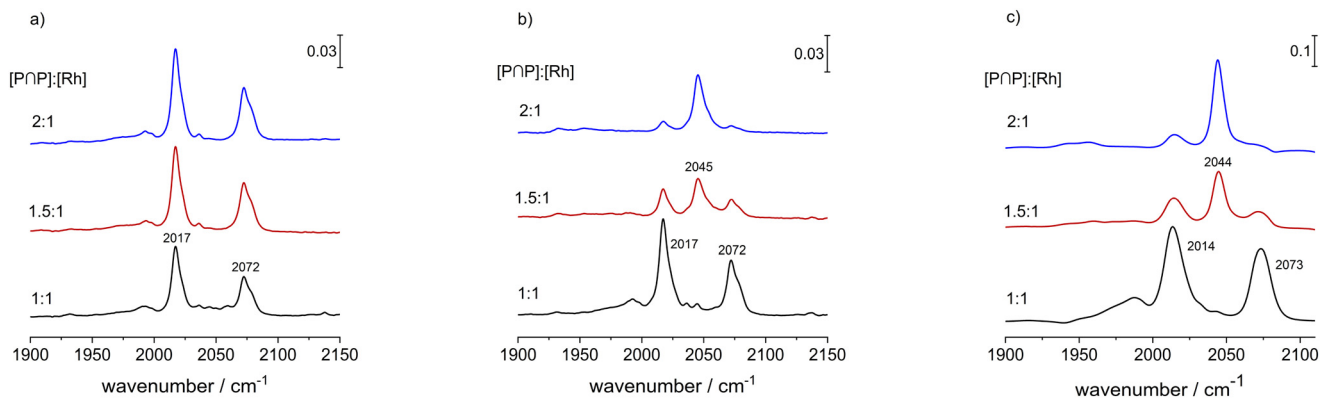

Fig. 18 Impact of ligand-to-metal ratio on the composition of hydrido complexes. a) [Rh] = 1 mM, ϑ = 90 °C, p(CO/H$_2$) = 2.0 MPa, solvent: cyclohexane; b) [Rh] = 1 mM, ϑ = 90 °C, p(H$_2$) = 1.0 MPa after repeated gas exchange cycles, solvent: cyclohexane; c) [Rh] = 20 mM, ϑ = 25 °C, p(H$_2$) = 0.1 MPa after repeated gas exchange cycles, solvent: toluene-d$_8$.

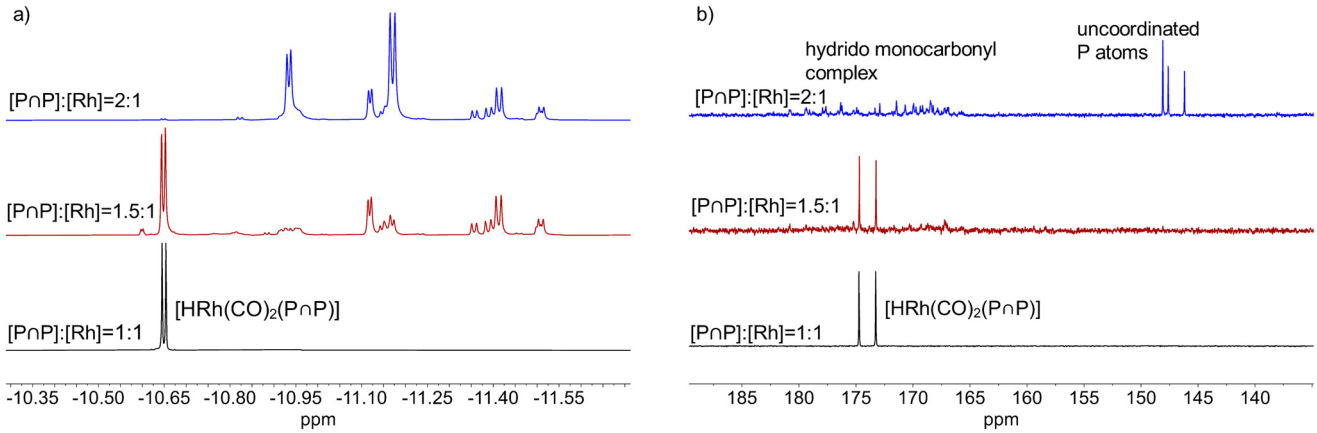

Fig. 19 a) $^{1}H\{^{31}P\}$-NMR and b) $^{31}P\{^{1}H\}$-NMR spectra of rhodium hydride complexes in H_2 atmosphere under varation of the ligand concentration (conditions: [Rh] = 20 mM, $p(H_2)$ = 0.1 MPa, ϑ = 25 °C, solvent: toluene-d_8).

The normalized integral values of the signals in both frequency regions are 2 : 1. It was also observed in the ^{1}H and ^{31}P-NMR spectra that the relative signal intensities for $[HRh(CO)_2(P\cap P)]$ decreased considerably. We conclude from these findings the formation of a mononuclear complex of the type $[HRh(CO)(P\cap P)(\kappa^1\text{-}P\cap P)]$ with one non-coordinated phosphorus atom (Scheme 6).[60–63] The coupled multiplets result from magnetic inequivalent P-atoms and atropisomerism.[45,64–66] A $^{1}H\{^{31}P\}$–^{103}Rh HMQC spectrum (Fig. 20) of this sample illustrates the involvement of several isomeric complexes. A conclusive structural assessment was impossible, but the similarity of the rhodium shifts (Fig. 20) makes a very similar coordination sphere likely.

In the next step, we conducted a H/D-isotope exchange experiment and a respective vibrational mode analysis based on DFT calculations for $[HRh(CO)(P\cap P)(\kappa^1\text{-}P\cap P)]$ to confirm the coordination mode of the phosphorus centers (Fig. 21) in the hydrido complex. For the deuterido complex a shift towards lower wavenumbers (ν(CO) = 2027 cm^{-1}) was observed, which is in accordance with a tris-equatorial coordination of the three phosphite units.

The formation of *e*,*e*,*e*-$[HRh(CO)(P\cap P)(\kappa^1\text{-}P\cap P)]$ with all three P-atoms coordinated in the equatorial position is likely due to sterical reasons. There are examples of *e*,*e*,*e*-$[HRh(CO)(P\cap P)L]$ complexes ($(P\cap P)$ = diphosphite, L = PPh_3, PPh_2R) with this type of coordination behavior of the P-ligands in the literature.[45,64] We prepared these type of complexes within the framework of this work with (L = PPh_3 and $P(OPh)_3$) and $^{31}P\{^{1}H\}$- and the ^{1}H-NMR spectra indicated a trisequatorial P-coordination (ESI-G†).

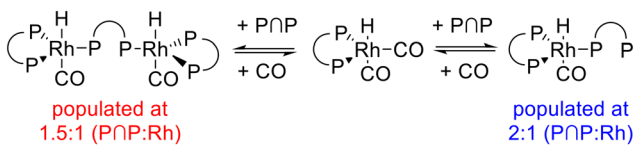

Scheme 6 Reaction of $[HRh(CO)_2(P\cap P)]$ with $[P\cap P]$ (BiPhePhos) in CO depleted atmosphere.

2.7 Formation and characterization of acyl complexes of the type $[RC(O)Rh(CO)_2(P\cap P)]$

For the Rh/BiPhePhos system under catalytic reaction conditions the only detectable resting state complex is the hydrido complex $[HRh(CO)_2(P\cap P)]$. This observation can be rationalized when considering the rate control in the catalytic cycle. In the literature on hydroformylation catalysts modified with bidentate diphosphites, kinetic and spectroscopic data are reported which are in accordance with a rate control located at steps early in the catalytic cycle (CO-dissociation, alkene coordination and alkene insertion).[45,67] Nevertheless, based on the established catalytic cycle, the 16 VE acyl complex is a crucial intermediate which is involved in the hydrogenolytic product formation step. In the presence of carbon monoxide, the equilibrium between the 16 and 18 VE acyl complexes lies generally far on the side of the electronically and coordinatively saturated complex.[68]

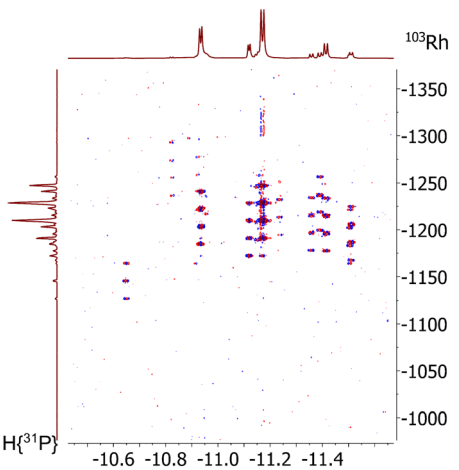

Fig. 20 $^{1}H\{^{31}P\}$–^{103}Rh-HMQC spectrum of stereoisomeric mixture of $[HRh(CO)(P\cap P)(\kappa^1\text{-}P\cap P)]$ type complex. Conditions: [Rh] = 20 mM, $[P\cap P]/[Rh]$ = 2, $p(H_2)$ = 0.1 MPa, ϑ = 25 °C, solvent: toluene-d_8. Most correlation signals appear quartet-like along F_1 as they represent RhP_3 species, and the ^{103}Rh–^{31}P coupling is observed in this dimension. Note: the triplet signal at −1146 ppm is due to $[HRh(CO)_2(P\cap P)]$.

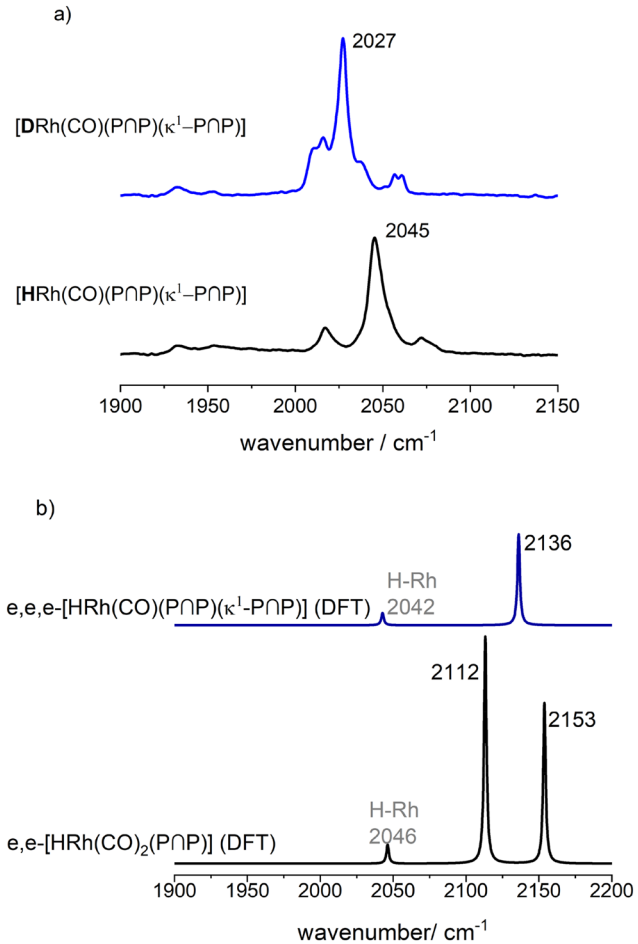

Fig. 21 a) Infrared spectra of the hydrido and deuterido monocarbonyl complex of the type [HRh(CO)(P∩P)(κ¹-P∩P)] for [Rh] = 1 mM and [P∩P] = 2 mM at $p(H_2/D_2)$ = 0.1 MPa, ϑ = 25 °C, solvent: cyclohexane; b) calculated vibrational spectra *via* DFT methods (ESI-I†) based on the molecular structures with trisequatorial P-coordination.

Ethene as substrate. In this work we combined the usage of ethene as the sterically least demanding alkene and the depletion of hydrogen to suppress the hydrogenolysis step to populate the 18 VE acyl complex(es) (Scheme 7) under pure CO atmosphere for its characterization *via in situ* IR- and high-pressure NMR-spectroscopy.[69]

In the first step the hydrido complex $[HRh(CO)_2(P\cap P)]$ was formed at catalytic conditions ([Rh] = 1 mM, [P∩P] = 1 mM, $p(CO/H_2)$ = 2.0 MPa and ϑ = 90 °C) in cyclohexane as solvent. Then the temperature was adjusted to ϑ = 30 °C

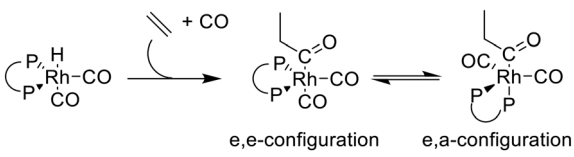

Scheme 7 Simplified reaction scheme for the formation of stereoisomeric acyl complexes with ethene as substrate.

and the gas atmosphere was exchanged several times by pure carbon monoxide. In the next step, 1.0 MPa of ethene was added into the reactor. During this treatment new carbonyl vibrational bands (ν(CO) = 1670, 1995, 2061 cm^{-1}) (Fig. 22a and ESI-H†) evolved while the bands ascribed to the hydrido complex completely vanished. The band at 1670 cm^{-1} lies in the spectral region expected for rhodium-acyl groups and the other bands at 1995 and 2061 cm^{-1} indicate two terminal carbonyl ligands.[68–73] These spectral features would be in agreement with an acyl complex of the type $[CH_3CH_2C(O)Rh(CO)_2(P\cap P)]$. We conducted a similar experiment at higher rhodium concentrations ([Rh] = 20 mM, [P∩P]/[Rh] = 1) in toluene-d_8 and the spectroscopic characteristics are comparable (Fig. 22b). Minor differences were observed such as the absence of smaller band contributions at 1677, 1983 and 2048 cm^{-1} observed in the experiment at [Rh] = 1 mM which stems probably from the solvent cyclohexane.

DFT calculations of infrared spectra have been performed to elucidate the ligand coordination in stereoisomeric acyl complexes. The relative band intensity patterns for the stereoisomers *e,e*- and *e,a*-$[CH_3CH_2C(O)Rh(CO)_2(P\cap P)]$ obtained from vibrational mode analysis have been compared to those of the experimental spectra. The experimental spectrum for the acyl complex shows an intensity ratio between both IR bands ($I[\nu(1995\ cm^{-1})]$/$I[\nu(2061\ cm^{-1})]$) of ≈1.9 : 1 (1 mM). Based on the calculated spectra *via* DFT methods an intensity ratio for corresponding band contributions of ≈1.6 : 1 for the *e,a*-isomer and of ≈1.1 : 1 for the *e,e*-isomer was obtained. This might indicate that the *e,a*-propionyl complexes has been formed preferentially. The relative energies of *e,e*- and *e,a*-propionyl complexes obtained from DFT computations give rise to a mixture of both stereoisomers with strong preference to the *e,a*-complex (ESI-J†). However, both stereoisomers have been formed which was investigated in the next step by NMR-spectroscopy.

HP NMR-spectroscopy of a solution prepared in toluene-d_8 ([Rh] = 20 mM, [P∩P]/[Rh] = 1) was performed for further investigations on the molecular structure of this complex. The advantage of this method is, among others, the possibility to measure the coupling constants between ^{13}C (acyl carbon) and ^{31}P (phosphite ligand) directly after an isotopic labeling with ^{13}CO (100%). A coupling constant larger than $^2J_{C,P}$ = ≥100 Hz indicates an *e,a*-ligand arrangement.[46] In contrast, the coupling constant for an *e,e*-arrangement is significantly smaller or in some cases not detectable.[6,41,44] The $^{13}C\{^1H\}$-NMR spectrum of this sample showed two broad signals in the spectral region of acyl groups ($\delta(^{13}C)$ = 210–235 ppm) at room temperature, that became sharper when the temperature was reduced (Fig. 23a).[69,72–75] This points to occurring intra- and intermolecular exchange processes. The acyl signal at $\delta(^{13}C)$ = 224.5 ppm appeared as a triplet of doublets at 273 K. When the temperature was further decreased to 223 K the slow exchange region was

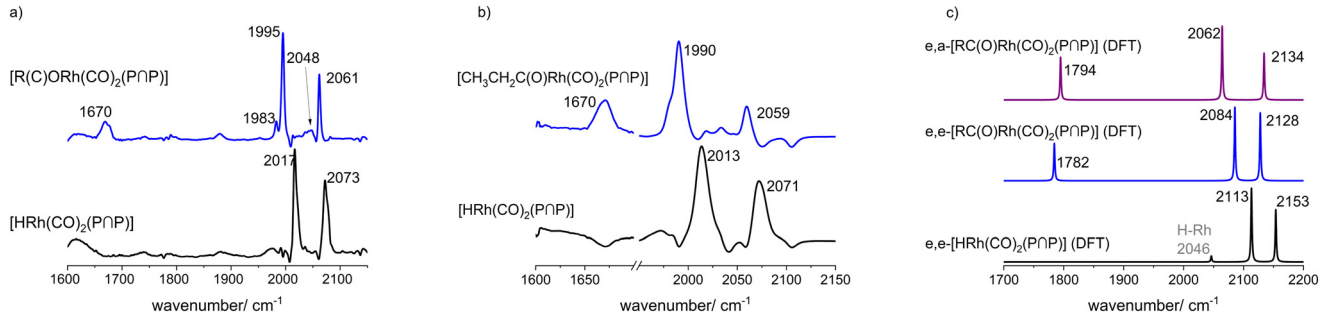

Fig. 22 Comparison between the *in situ* IR-spectra of $[HRh(CO)_2(P\cap P)]$ and $[CH_3CH_2C(O)Rh(CO)_2(P\cap P)]$ a) at lower Rh concentrations ([Rh] = 1 mM, solvent: cyclohexane), b) at higher Rh concentrations ([Rh] = 20 mM, solvent: toluene) and c) DFT-based IR-spectra (ESI-I†) of the *e,a*- and *e,e*-acyl complexes and *e,e*-$[HRh(CO)_2(P\cap P)]$. Experimental conditions: ϑ = 30 °C, [Rh]/[P∩P] = 1, p(CO) = 1.0 MPa, $p(C_2H_4)$ = 1.0 MPa.

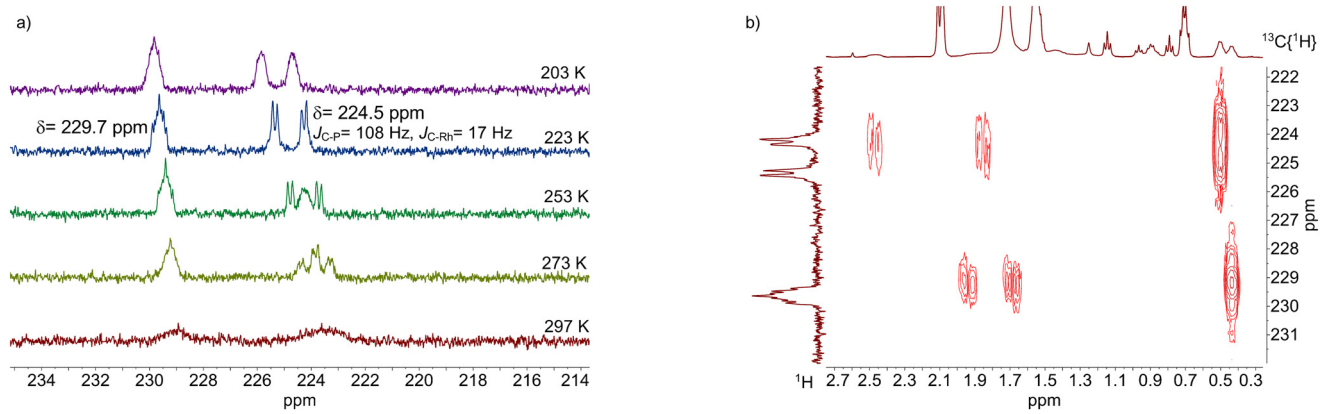

Fig. 23 $^{13}C\{^1H\}$-NMR (a) and ^1H–^{13}C-HMBC-NMR (b) spectra of stereoisomeric acyl complexes in a 5 mm sapphire tube after ^{13}CO labeling. Conditions: [Rh] = 20 mM, [P∩P] = 20 mM, $p(^{13}CO)$ = 1.0 MPa, $p(C_2H_4)$ = 1.0 MPa, solvent: toluene-d_8.

achieved and the acyl signal appeared as a doublet of doublets ($^1J_{C,Rh}$ = 16 Hz, $^2J_{C,P}$ = 106 Hz). The large C–P coupling indicates an *e,a*-arrangement of the P-atoms. The second signal at $\delta(^{13}C)$ = 229.7 ppm was characterized by a complex multiplet patterns with a small C–P coupling. This suggests a second acyl complex with an *e,e*-arrangement.

Due to the different sterical properties the two isomeric acyl complexes should show up different chemical shifts for the propionyl group bonded to the rhodium centre. A ^1H–$^{13}C\{^1H\}$-HMBC spectrum measured at 223 K allowed us to confirm this anticipation. The HMBC-spectrum showed overall six correlation signals for the two acyl complexes (Fig. 23b). The signal at $\delta(^{13}C)$ = 229.7 ppm corresponding to the *e,e*-acyl complex correlates with a signal at $\delta(^1H)$ = 0.4 ppm, which is caused by a CH_3-group. Other two cross-peaks for the rhodium-acyl signal at $\delta(^{13}C)$ = 229.7 ppm and signals at $\delta(^1H)$ = 1.7 and 2 ppm, reveal the two nonequivalent protons of the α-CH_2 group due to the distorted symmetry. The HMBC-spectrum showed also comparable cross-peaks for the *e,a*-acyl complex. The signal at $\delta(^{13}C)$ = 229.7 ppm correlates with the signal at $\delta(^1H)$ = 0.5 ppm (CH_3-group) as well as with $\delta(^1H)$ = 1.9 and 2.5 ppm (nonequivalent protons of the α-CH_2 group). Based on the correlation peaks between these CH_3-groups and the acyl signals in the ^{13}C-spectrum we were able to distinguish both complexes qualitatively.

The $^{31}P\{^1H\}$-NMR spectra showed a very complex fine splitting due to the coupling between the ^{31}P, ^{13}C and ^{103}Rh atoms. Regarding the complex structure and the molar ratios between the isomeric complexes of this sample no information was derived but clarification was achieved with a sample based on neohexene as alkene.

Neohexene as substrate. We were interested to use a sterically more demanding alkene for the formation of an acyl complex under hydrogen depleted gas atmosphere. A similar experimental protocol was followed to form first the hydrido complex $[HRh(CO)_2(P\cap P)]$ at the bench-mark conditions ([Rh] = 1 mM, [P∩P] = 1 mM, ϑ = 90 °C, $p(H_2)$ = 1.0 MPa and p(CO) = 1.0 MPa). After lowering the temperature to 30 °C, the gas atmosphere was substituted by pure carbon monoxide (1.0 MPa) and then neohexene was added *via* a syringe pump. The infrared spectrum of the newly formed

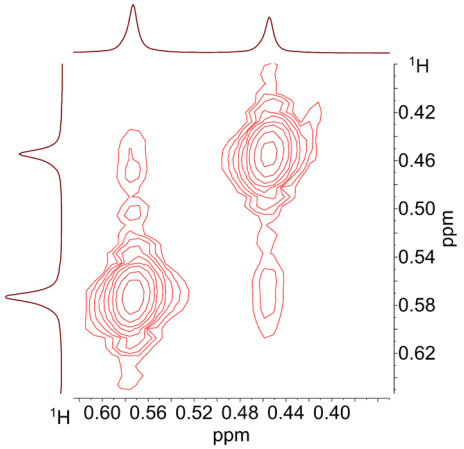

Fig. 24 ^{1}H–^{1}H-EXSY spectrum of the equilibrium between *e*,*a*- and *e*,*e*-[RC(O)Rh(CO)$_2$(P∩P)] complexes at 253 K. Further conditions: [Rh] = 20 mM, [P∩P] = 20 mM, [neohexene] = 80 mM, *p*(CO) = 0.1 MPa, solvent: toluene-d$_8$.

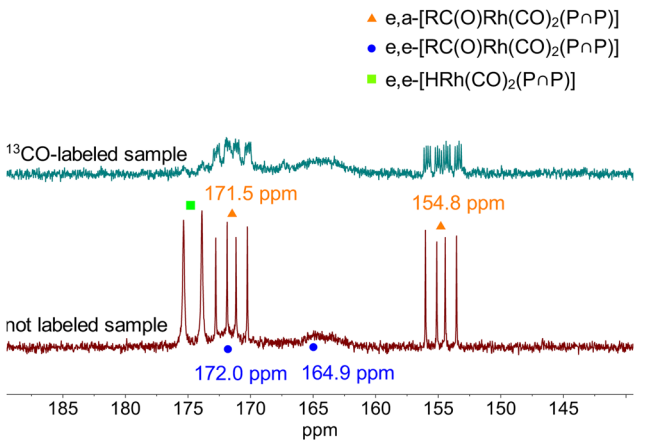

Fig. 25 ^{31}P{^{1}H}-NMR spectra of *e*,*a*- and *e*,*e*-[RC(O)Rh(CO)$_2$(P∩P)] complexes at 253 K (bottom: without ^{13}C-labeling and top: after ^{13}CO labeling). Further conditions: [Rh] = 20 mM, [P∩P] = 20 mM, [neohexene] = 80 mM, *p*(CO) = 0.1 MPa, solvent: toluene-d$_8$.

species showed identical spectral features found for the propionyl complex with band contributions at ν(CO) = 1670, 1995, 2061 cm^{-1} assigned to an acyl complex of the type [RC(O)Rh(CO)$_2$(P∩P)] (ESI-H†).

For further NMR-spectroscopic characterizations a sample with [Rh] = 20 mM and [P∩P]/[Rh] = 1 was prepared in toluene-d$_8$ and labeled with ^{13}CO. It was found that the spectroscopic characteristics did not change when the CO pressure was adjusted to 0.1 MPa which made the NMR analyses using a Young-NMR-tube possible with an improved spectra quality. ^{13}C{^{1}H}-NMR-measurements on this sample under variation of the temperature (298 to 203 K) showed again the formation of the two stereoisomeric *e*,*e*-/*e*,*a*-acyl complexes (ESI-H†). Cooling to 223 K of the sample lead to distinct signal patterns with a resolved doublet of doublet shape for the *e*,*a*-acyl complex. Corresponding CH-groups of the neohexyl moiety could be determined *via* a ^{1}H–^{13}C-HMBC spectrum at 253 K (ESI-H†). The *tert*-butyl groups for both complexes are located around 0.4 to 0.6 ppm in the ^{1}H-NMR spectrum. To obtain further information regarding a possible intramolecular equilibrium of the acyl complexes in solution we conducted an additional ^{1}H–^{1}H-NOESY (EXSY) NMR experiment revealing an exchange of the –C(CH$_3$)$_3$-groups (Fig. 24). This result is in line with a dynamic interconversion of the configurational isomeric acyl complexes.[72] The NMR data gave indications for a preferred formation of the *e*,*a*-isomer. Based on DFT computations also the *e*,*a*-complex is thermodynamically more stable for the investigated temperatures (ESI-J†).

In addition, we investigated the ^{31}P{^{1}H}-NMR spectrum for further details (Fig. 25). The usage of a ^{13}CO labeled sample revealed two doublet signals of which one doublet shows a dddd fine splitting. This multiplet splitting is caused by the coupling between the ^{31}P, ^{103}Rh and ^{13}C atoms. The ^{31}P{^{1}H}-NMR spectrum of a non ^{13}CO-labeled sample and lower neohexene concentrations simplified the study towards an assignment of the signals to the respective stereoisomeric structures of the acyl complexes. The signal set with the observed fine splitting δ(^{31}P) = 154.8 ppm ($^1J_{P,Rh}$ = 262 Hz) and 171.5 ppm ($^1J_{P,Rh}$ = 255 Hz) with a P–P coupling of $^2J_{P,P}$ = 147 Hz is in accordance with the *e*,*a*-complex. The two broad signals showing no distinct fine splitting at δ(^{31}P) = 164.9 and 172.0 ppm were assigned to the *e*,*e*-acyl complex.

3. Conclusions

Rhodium complexes modified with the chelating diphosphite BiPhePhos were characterized by *in situ* HP IR and NMR-spectroscopy. The hydrido complex *e*,*e*-[HRh(CO)$_2$(P∩P)] is the only observable resting state complex at conditions typical for hydroformylation. The hydrido complex is relatively stable in solution in the absence of hydrogen or synthesis gas and dinuclear complexes appear to form only after prolonged treatments at higher temperatures. In the presence of air the hydrido complex and the diphosphite are decomposed at elevated temperatures. [HRh(CO)$_2$(P∩P)] and BiPhePhos show hydrolytic decomposition when exposed to water. The increase of the [P∩P]/[Rh] ratio to 1.5 and 2 leads to the formation of monocarbonyl complexes in CO-depleted atmospheres. One of these complexes is a ligand bridging hydrido complex (*e*,*e*,*e*-[HRh(CO)(P∩P)]$_2$(P∩P)) and the other is the corresponding monomer [HRh(CO)(P∩P)(κ^1-P∩P)] with an uncoordinated phosphite moiety. The population of acyl complexes of the type [RC(O)Rh(CO)$_2$(P∩P)] is possible in H$_2$ impoverished gas atmospheres with ethene and neohexene as alkenes. Two stereoisomers with *e*,*e*- and *e*,*a*-coordinations of both P-atoms are present in a chemical equilibrium. In Fig. 26 an overview is presented on the various rhodium carbonyl complexes being parts of a larger network of interconvertible species.

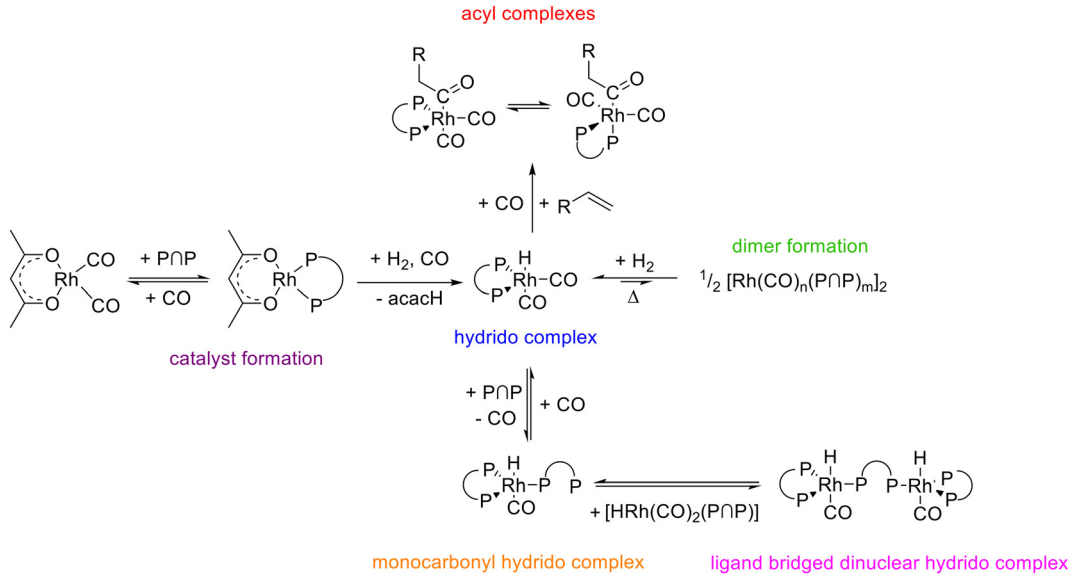

Fig. 26 Summary of the interconversions between diphosphite (BiPhePhos) modified rhodium complexes in the alkene hydroformylation.

Experimental and computational section

Further supplementary data and details on the laboratory experiments and computations are given in the ESI.†

Data availability

The respective data supporting the findings of this research study is given as figures/tables of spectra and concentration–time-data in the main manuscript and in the ESI.† Original and processed data available in specific data formats can be provided on request from the corresponding author.

Conflicts of interest

The authors declare no conflicts of interest.

Acknowledgements

Jiali Liu thanks the European Union's Horizon 2020 research and innovation programme under the Marie Sklodowska-Curie grant agreement No. 859910. Christoph Kubis is thankful for the DFG Research Unit FOR 5538 IMPD4Cat (Project No. 501735683).

References

1 R. Franke and A. Börner, *Hydroformylation: Fundamentals, Processes, and Applications in Organic Synthesis*, Wiley-VCH, Weinheim, 2016.
2 R. Franke, D. Selent and A. Börner, Applied Hydroformylation, *Chem. Rev.*, 2012, **112**, 5675–5732.
3 *Homogeneous Catalysis with Organometallic Compounds*, ed. B. Cornils, W. A. Herrmann, M. Beller and R. Paciello, Wiley-VCH, Weinheim, 3rd edn, 2018.
4 *Rhodium Catalyzed Hydroformylation*, ed. P. W. N. M. van Leeuwen and C. Claver, Kluwer, Dordrecht, 2002.
5 P. W. N. M. van Leeuwen and J. C. Chadwick, *Homogeneous Catalysts*, Wiley-VCH, Weinheim, 2011.
6 D. Selent, R. Franke, C. Kubis, A. Spannenberg, W. Baumann, B. Kreidler and A. Börner, *Organometallics*, 2011, **30**, 4509–4514.
7 P. P. Deutsch and R. Eisenberg, *Organometallics*, 1990, **9**, 709–718.
8 A. B. Permin and R. Eisenberg, *J. Am. Chem. Soc.*, 2002, **124**, 12406–12407.
9 D. Guan, C. Godard, S. M. Polas, R. P. Tooze, A. C. Whitwood and S. B. Duckett, *Dalton Trans.*, 2019, **48**, 2664–2675.
10 M. Garland and P. Pino, *Organometallics*, 1991, **10**, 1693–1704.
11 A. van Rooy, E. N. Orij, P. C. J. Kamer and P. W. N. M. van Leeuwen, *Organometallics*, 1995, **14**, 34–43.
12 S. C. van der Slot, P. C. J. Kamer, P. W. N. M. van Leeuwen, J. A. Iggo and B. T. Heaton, *Organometallics*, 2001, **20**, 430–441.
13 O. Diebolt, P. W. N. M. van Leeuwen and P. C. J. Kamer, *ACS Catal.*, 2012, **2**, 2357–2370.
14 M. Garland, in *Mechanisms in Homogeneous Catalysis*, ed. B. Heaton, Wiley-VCH, Weinheim, 2005, pp. 151–193.
15 M. Garland, *Catal. Today*, 2010, **155**, 266–270.
16 C. Li, E. Widjaja, W. Chew and M. Garland, *Angew. Chem., Int. Ed.*, 2002, **41**, 3785–3789.
17 B. Moasser, W. L. Gladfelter and D. C. Roe, *Organometallics*, 1995, **14**, 3832–3838.
18 A. Behr, D. Obst, C. Schulte and T. Schosser, *J. Mol. Catal. A: Chem.*, 2003, **206**, 179–184.
19 A. Behr, D. Obst and C. Schulte, *Chem. Ing. Tech.*, 2004, **76**, 904–910.
20 C. Vogl, E. Paetzold, C. Fischer and U. Kragl, *J. Mol. Catal. A: Chem.*, 2005, **232**, 41–44.

21 A. Jörke, A. Seidel-Morgenstern and C. Hamel, *J. Mol. Catal. A: Chem.*, 2017, **426**, 10–14.
22 A. Jörke, T. Gaide, A. Behr, A. Vorholt, A. Seidel-Morgenstern and C. Hamel, *Chem. Eng. J.*, 2017, **313**, 382–397.
23 J. M. Dreimann, E. Kohls, H. F. W. Warmeling, M. Stein, L. F. Guo, M. Garland, T. N. Dinh and A. J. Vorholt, *ACS Catal.*, 2019, **9**, 4308–4319.
24 T. Gaide, A. Jörke, K. E. Schlipköter, C. Hamel, A. Seidel-Morgenstern, A. Behr and A. J. Vorholt, *Appl. Catal., A*, 2017, **532**, 50–56.
25 G. Kiedorf, D. M. Hoang, A. Müller, A. Jörke, J. Markert, H. Arellano-Garcia, A. Seidel-Morgenstern and C. Hamel, *Chem. Eng. Sci.*, 2014, **115**, 31–48.
26 J. M. Dreimann, M. Skiborowski, A. Behr and A. J. Vorholt, *ChemCatChem*, 2016, **8**, 3330–3333.
27 A. Lejeune, L. Le Goanvic, T. Renouard, J.-L. Couturier, J.-L. Dubois, J.-F. Carpentier and M. Rabiller-Baudry, *ChemPlusChem*, 2019, **84**, 1744–1760.
28 M. Haumann, M. Jakuttis, R. Franke, A. Schönweiz and P. Wasserscheid, *ChemCatChem*, 2011, **3**, 1822–1827.
29 S. Walter, H. Spohr, R. Franke, W. Hieringer, P. Wasserscheid and M. Haumann, *ACS Catal.*, 2017, **7**, 1035–1044.
30 M. Logemann, J. M. Marinkovic, M. Schörner, E. José García-Suárez, C. Hecht, R. Franke, M. Wessling, A. Riisager, R. Fehrmann and M. Haumann, *Green Chem.*, 2020, **22**, 5691–5700.
31 C. Li, K. Xiong, L. Yan, M. Jiang, X. Song, T. Wang, X. Chen, Z. Zhan and Y. Ding, *Catal. Sci. Technol.*, 2016, **6**, 2143–2149.
32 C. Li, L. Yan, L. Lu, K. Xiong, W. Wang, M. Jiang, J. Liu, X. Song, Z. Zhan, Z. Jiang and Y. Ding, *Green Chem.*, 2016, **18**, 2995–3005.
33 Y. Wang, L. Yan, C. Li, M. Jiang, W. Wang and Y. Ding, *Appl. Catal., A*, 2018, **551**, 98–105.
34 B. N. Leidecker, C. Kubis, A. Spannenberg, R. Franke and A. Börner, *IUCrData*, 2019, **4**, x191636.
35 R. A. Alberty and C. A. Gehrig, *J. Phys. Chem. Ref. Data*, 1985, **14**, 803–820.
36 F. G. Helfferich, Kinetics of Multistep Reactions, in *Comprehensive Chemical Kinetics*, ed. N. J. B. Green, Elsevier Science, Amsterdam, 2nd edn, 2004, vol. 40.
37 C. Kubis, R. Ludwig, M. Sawall, K. Neymeyr, A. Börner, K.-D. Wiese, D. Hess, R. Franke and D. Selent, *ChemCatChem*, 2010, **2**, 287–295.
38 **https://www.math.uni-rostock.de/facpack/**.
39 M. Sawall, C. Kubis, E. Barsch, D. Selent, A. Börner and K. Neymeyr, *J. Iran. Chem. Soc.*, 2016, **13**, 191–205.
40 H. Schröder, M. Sawall, C. Kubis, A. Jürß, D. Selent, A. Brächer, A. Börner, R. Franke and K. Neymeyr, *Chemom. Intell. Lab. Syst.*, 2017, **163**, 55–63.
41 A. Bara-Estaún, C. L. Lyall, J. P. Lowe, P. G. Pringle, P. C. J. Kamer, R. Franke and U. Hintermair, *ChemCatChem*, 2023, **15**, e202201204.
42 L. Vaska, *J. Am. Chem. Soc.*, 1966, **88**, 4100–4101.
43 C. Kubis, M. König, B. N. Leidecker, D. Selent, H. Schröder, M. Sawall, W. Baumann, A. Spannenberg, A. Brächer, K. Neymeyr, R. Franke and A. Börner, *ACS Catal.*, 2023, **13**, 5245–5263.
44 A. van Rooy, P. C. J. Kamer, P. W. N. M. van Leeuwen, K. Goubitz, J. Fraanje, N. Veldman and A. L. Spek, *Organometallics*, 1996, **15**, 835–847.
45 A. Bara-Estaún, *PhD thesis*, University of Bath, 2022.
46 P. C. J. Kamer, J. N. H. Reek and P. W. N. M. van Leeuwen, in *Mechanism in Homogeneous Catalysis*, ed. B. Heaton, Wiley-VCH, Weinheim, 2005, pp. 231–269.
47 G. J. H. Buisman, L. A. van der Veen, P. C. J. Kamer and P. W. N. M. van Leeuwen, *Organometallics*, 1997, **16**, 5681–5687.
48 A. Castellanos-Páez, S. Castillón, C. Claver, P. W. N. M. van Leeuwen and W. G. J. de Lange, *Organometallics*, 1998, **17**, 2543–2552.
49 P. Meakin, E. L. Muetterties and J. P. Jesson, *J. Am. Chem. Soc.*, 1972, **94**, 5271–5285.
50 R. S. Berry, *J. Chem. Phys.*, 1960, **32**, 933–938.
51 L. A. van der Veen, P. C. J. Kamer and P. W. N. M. van Leeuwen, *Organometallics*, 1999, **18**, 4765–4777.
52 L. A. van der Veen, P. H. Keeven, G. C. Schoemaker, J. N. H. Reek, P. C. J. Kamer, P. W. N. M. van Leeuwen, M. Lutz and A. L. Spek, *Organometallics*, 2000, **19**, 872–883.
53 P. W. N. M. van Leeuwen, *Appl. Catal., A*, 2001, **212**, 61–81.
54 K. Köhnke, N. Wessel, J. Esteban, J. Jin, A. J. Vorholt and W. Leitner, *Green Chem.*, 2022, **24**, 1951–1972.
55 M. Gerlach, F. Jameel, A. Seidel-Morgenstern, M. Stein and C. Hamel, *Catal. Sci. Technol.*, 2023, **13**, 1788–1801.
56 B. Zhang, H. Jiao, D. Michalik, S. Kloß, L. M. Deter, D. Selent, A. Spannenberg, R. Franke and A. Börner, *ACS Catal.*, 2016, **6**, 7554–7565.
57 S. Kloß, D. Selent, A. Spannenberg, R. Franke, A. Börner and M. Sharif, *Catalysts*, 2019, **9**, 1036.
58 U. Nettekoven, P. C. J. Kamer, M. Widhalm and P. W. N. M. van Leeuwen, *Organometallics*, 2000, **19**, 4596–4607.
59 E. Zuidema, P. E. Goudriaan, B. H. G. Swennenhuis, P. C. J. Kamer, P. W. N. M. van Leeuwen, M. Lutz and A. L. Spek, *Organometallics*, 2010, **29**, 1210–1221.
60 S. C. van der Slot, J. Duran, J. Luten, P. C. J. Kamer and P. W. N. M. van Leeuwen, *Organometallics*, 2002, **21**, 3873–3883.
61 Z. Freixa and J. Carles Bayón, *J. Chem. Soc., Dalton Trans.*, 2001, 2067–2068.
62 O. R. Hughes and D. A. Young, *J. Am. Chem. Soc.*, 1981, **103**, 6636–6642.
63 B. N. Leidecker, A. Spannenberg, R. Franke, A. Borner and C. Kubis, *IUCrData*, 2023, **8**, x230083.
64 A. van Rooy, P. C. J. Kamer and P. W. N. M. van Leeuwen, *J. Organomet. Chem.*, 1997, **535**, 201–207.
65 J. R. Briggs and G. T. Whiteker, *Chem. Commun.*, 2001, 2174–2175.
66 R. Franke, C. Borgmann, D. Hess and K.-D. Wiese, *Z. Anorg. Allg. Chem.*, 2003, **629**, 2535–2538.
67 E. Zuidema, L. Escorihuela, T. Eichelsheim, J. J. Carbo, C. Bo, P. C. Kamer and P. W. van Leeuwen, *Chem. – Eur. J.*, 2008, **14**, 1843–1853.

68 C. Kubis, M. Sawall, A. Block, K. Neymeyr, R. Ludwig, A. Börner and D. Selent, *Chem. – Eur. J.*, 2014, **20**, 11921–11931.
69 J. M. Brown and A. G. Kent, *J. Chem. Soc., Perkin Trans. 2*, 1987, 1597–1607.
70 C. Kubis, D. Selent, M. Sawall, R. Ludwig, K. Neymeyr, W. Baumann, R. Franke and A. Börner, *Chem. – Eur. J.*, 2012, **18**, 8780–8794.
71 G. Liu, R. Volken and M. Garland, *Organometallics*, 1999, **18**, 3429–3436.
72 S. C. van der Slot, P. C. J. Kamer, P. W. N. M. van Leeuwen, J. A. Iggo and B. T. Heaton, *Organometallics*, 2001, **20**, 430–441.
73 S. Güven, M. M. L. Nieuwenhuizen, B. Hamers, R. Franke, M. Priske, M. Becker and D. Vogt, *ChemCatChem*, 2014, **6**, 603–610.
74 E. R. Nelsen and C. R. Landis, *J. Am. Chem. Soc.*, 2013, **135**, 9636–9639.
75 P. Dingwall, J. A. Fuentes, L. E. Crawford, A. M. Z. Slawin, M. Bühl and M. L. Clarke, *J. Am. Chem. Soc.*, 2017, **139**, 15921–15932.